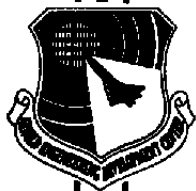# Liquid Film Cooling in Rocket Engines

William M. Grisson
Physics Department
Morehouse College
Atlanta, Georgia 30314

March 1991

Final Report for Period June 1987 to December 1989

TECHNICAL REPORTS
FILE COPY

**ARNOLD ENGINEERING DEVELOPMENT CENTER
ARNOLD AIR FORCE BASE, TENNESSEE
AIR FORCE SYSTEMS COMMAND
UNITED STATES AIR FORCE**

This report has been reviewed by the Office of Public Affairs (PA) and is releasable to the National Technical Information Service (NTIS). At NTIS, it will be available to the general public, including foreign nations.

APPROVAL STATEMENT

This report has been reviewed and approved.

PAUL LACASSE, Capt, CF
Facility Technology Division
Directorate of Technology
Deputy for Operations

Approved for publication:

FOR THE COMMANDER

KEITH L. KUSHMAN
Technical Director
Directorate of Technology
Deputy for Operations

REPORT DOCUMENTATION PAGE

1 AGENCY USE ONLY (Leave blank)	2. REPORT DATE **March 1991**	3 REPORT TYPE AND DATES COVERED **Final, June 1987 - March 1989**

4. TITLE AND SUBTITLE	5. FUNDING NUMBERS
Liquid Film Cooling in Rocket Engines	**F49620-85-C-0013**

6. AUTHOR(S)

Grissom, William M., Morehouse College

7 PERFORMING ORGANIZATION NAME(S) AND ADDRESS(ES)	8. PERFORMING ORGANIZATION REPORT NUMBER
William M. Grissom **Physics Department** **Morehouse College** **Atlanta, GA 30314**	**AEDC-TR-91-1**

9. SPONSORING/MONITORING AGENCY NAMES(S) AND ADDRESS(ES)	10. SPONSORING/MONITORING AGENCY REPORT NUMBER
Arnold Engineering Development Center/DO **Air Force Systems Command** **Arnold AFB, TN 37389-5000**	

11 SUPPLEMENTARY NOTES

Available in Defense Technical Information Center (DTIC).

12a DISTRIBUTION/AVAILABILITY STATEMENT	12b. DISTRIBUTION CODE
Approved for public release; distribution is unlimited.	

13. ABSTRACT (Maximum 200 words)

A one-dimensional analytical model of liquid film cooling in rocket engine combustion chambers is developed and compared with existing data. The vapor generated at the liquid interface greatly decreases the convective heat flux and is treated as a "transpiration" process. The radiant heat is absorbed at the walls and transmitted to the liquid film by boiling, which can lead to burnout of the film. Downstream of the liquid film, the vapor provides continued thermal protection to the wall and is treated as a gaseous film cooling process. A standard correlation is expressed in differential form to allow for the nonuniform free-stream flow in the nozzle. Liquid film lengths are well predicted by the model. Downstream of the dry-out point, wall temperatures are well predicted up to the start of convergence. Downstream of the converging turn, a correction term, correlated by a "centrifugal parameter," is required to account for increased mixing at the converging turn. Downstream of the throat, wall temperatures decrease very quickly because of acceleration of the boundary-layer gases, an effect not included in the model.

14. SUBJECT TERMS		15. NUMBER OF PAGES **74**
liquid-propellant rocket motors transpiration liquid film cooling heat transfer gaseous film cooling		16 PRICE CODE

17 SECURITY CLASSIFICATION OF REPORT **UNCLASSIFIED**	18 SECURITY CLASSIFICATION OF THIS PAGE **UNCLASSIFIED**	19 SECURITY CLASSIFICATION OF ABSTRACT **UNCLASSIFIED**	20 LIMITATION OF ABSTRACT **SAME AS REPORT**

PREFACE

The research reported herein was sponsored by the Air Force Office of Scientific Research/AFSC under Contract F49620-85-C-0013/SB5851-0361 as a follow-on to work done in the summer of 1987 on the Universal Energy Systems Summer Faculty Research Program at Arnold Engineering Development Center, Arnold AFB, Tennessee. The author returned to AEDC during the summer of 1988 to continue work on the project. Appreciation is extended to C. C. Limbaugh and W. K. McGregor for suggesting the topic, to M. A. Simmons for running the NASA equilibrium code, and to Mike Powell of the Air Force Astronautics Laboratory for providing numerous references to rocket test reports. M. K. Kingery supervised the Summer Faculty program at AEDC.

The reproducibles used in this report were supplied by the author.

CONTENTS

ILLUSTRATIONS

1.0 INTRODUCTION

Many liquid rocket engines employ a film of liquid fuel as thermal protection for the combustion chamber walls. This process was experimentally studied in the 1950's and 1960's, however no general analysis was developed. Since then a number of fundamental heat transfer studies have been performed which allow the liquid film cooling problem to be analyzed as a collection of several fundamental processes.

The mechanisms involved in liquid film cooling are depicted in Figure 1. Heat is transferred from the hot free stream gas to the liquid film by both radiation and convection. This energy is absorbed in vaporizing the liquid in the protective film on the wall. The vapor generated flows outward from the liquid film, decreasing the normally expected convective heat flux by the well-known transpiration cooling process. Downstream of the liquid film the vapor mixes with the free stream gas entrained in the boundary layer, lowering the wall temperature through the well-known "gaseous film cooling" process. This provides thermal protection downstream of the dryout point.

The existing heat transfer correlations are for the flow of a low turbulence gas at constant velocity over a flat plate. These were extended to the case of developing, accelerating, and turbulent free stream flows. Since the goal was to develop a simple model, suitable for design and test analysis, only a simple one-dimensional model was considered.

2.0 LIQUID FILM EVAPORATION

2.1 CONVECTIVE HEAT TRANSFER

The flow over the combustion chamber walls is almost like that over a flat plate in a uniform free stream flow, the difference being that it arises from an effective stagnation point rather than an abrupt leading edge. However, for a turbulent boundary layer the exact starting conditions quickly become unimportant.

In the absence of the liquid film, the normal convective heat flux can be calculated using one of the many flat-plate data correlations (Reference 1). Most agree within 5%. One simple correlation with an analytical basis, termed "Colburn's Equation", is based upon a 1/7th power law velocity profile (Reference 2). Expressed in terms of the friction factor, C_f, and the Reynold's number based upon the distance x from the leading edge:

$$C_{fo} = 0.0592 \, Re_x^{-0.2} \qquad \text{(Equation 2.1)}$$

Using Reynold's momentum-heat analogy for turbulent convection, a non-dimensional heat transfer coefficient, the Stanton number, is expressed:

$$St_0 = \tfrac{1}{2} \, C_{fo} \, Pr^{-0.6} \qquad \text{(Equation 2.2)}$$

Colburn's Equation is applicable for $Re_x < 1.10^7$. In most rocket engines this condition is satisfied.

In a rocket engine there is a large temperature difference between the combustion gases and the liquid film, so that the temperature at which the properties are evaluated is important. It is common practice in boundary layer correlations to evaluate properties at the free stream gas temperature. A correction factor for the free stream to wall temperature ratio is then multiplied, the exponent being 0.26, 0.4, or 0.5 depending upon the author (References 3, 4, or 5, respectively). However, evaluating all of the properties at the mean temperature of the free stream and wall eliminates such correction factors, and is assumed here.

As the boundary layer grows, the cylindrical geometry becomes important. The most extensive measurements in fully-developed pipe flow at high temperatures were by Humble (Reference 6). He obtained a correlation which can be written (using Nu = StRePr):

$$St_0 = 0.023 \, Re_D^{-0.2} \, Pr^{-0.6} \qquad \text{(Equation 2.3)}$$

6

where the Reynold's number is based on the pipe diameter. Humble found that if the property values were evaluated at the mean temperature, then no temperature correction factor was necessary.

Bartz (Reference 7) found that Equation 2.3 predicted the heat flux at the throat of an RFNA/N_2F_4 rocket if the constant was 0.026 . In Bartz' tests the flow was not completely developed, which explains the slightly larger constant. This so-called "Bartz Equation" has been commonly used to calculate convective heat fluxes in rocket engines. Not surprisingly, it usually underpredicts the convective heat flux upstream of the throat where the assumption of fully-developed flow is not justified.

For $x > 3.53$ D the flat plate correlation (Equation 2.2) predicts a lower heat flux than that for fully-developed flow (Equation 2.3). Certainly the heat flux cannot fall below that for fully-developed flow. To patch these two limiting cases together, Equation 2.2 can be used, but with x replaced by an effective x_e (Reference 8):

$$x_e = 3.53 \ D \left[1 + \left[\frac{x}{3.53 \ D} \right]^{-m} \right]^{-1/m}$$

The exponent $m = 1.2$ gives the best comparison with the data of Barbin and Jones (Reference 9), as shown in Figure 2. Their data was taken at $Re_D = 388,000$ which is in the range of the data analyzed in Section 4.1. The optimum exponent is probably a function of the Reynold's number.

The convective heat flux for the flow of free stream gas over the dry walls of the combustion chamber is then calculated as:

$$\dot{Q}_{conv} = h_0 \Delta T$$

where $h_0 = G_{mean} C_{pg} St_0$. G_{mean} is the gas mass flow per area, evaluated at the mean temperature between the gas and liquid film. It is scaled from the chamber value (G_{ch}) as:

$$G_{mean} = G_{ch}(T_g/T_{mean})[(U_g - U_l)/U_g]$$

The second factor accounts for the velocity of the free stream relative to the liquid surface. The liquid surface velocity (U_l) is given in Section 2.2.2 .

2.1.1 Free-stream Turbulence

The convective heat flux increases by a factor $K_t = 1 + 4.0\,e_t$ in the presence of an rms turbulence fraction, e_t, in the free-stream flow (Reference 10).

Two studies measured the turbulence intensities in rocket engines. Hersch (Reference 11) found $e_t = 0.10$ to 0.05 at distances of 2 to 8 inches from the injector in a LOx/GH$_2$ engine, while Talmor (Reference 12) found $e_t = 0.20$ to 0.15 at distances of 6 to 23 inches from the injector in an N$_2$O$_4$/Az50 engine.

2.1.2 Transpiration Corrections

The total heat flux due to both convection and radiation, Q_{tot}, is absorbed in the liquid film, causing an initial temperature rise: $dT_{liq}/dx = Qtot/(\Gamma C_p)$, where Γ is the local liquid mass flow rate per circumference. After the liquid film reaches the saturation temperature, T_v, the evaporation rate per area is:

$$\dot{m}_v = \dot{Q}_{tot}/\lambda = (\dot{Q}_{conv} + \dot{Q}_{rad})/\lambda \qquad \text{(Equation 2.4)}$$

This vapor flows away from the liquid film, similar to gaseous transpiration through a porous wall. Transpiration decreases the wall shear stress and convective heat flux by a factor dependant upon the "blowing parameter": $F = \dot{m}_v/G$.

The simplest transpiration analysis assumes that the transpiring vapor does not change the thickness of the viscous sublayer in the boundary layer. Normally the velocity profile in the viscous sublayer is linear. With blowing, it becomes an exponential function. The ratio of the wall shear stress in the blown (τ_w) to unblown case (τ_{wo}) is:

$$\frac{\tau_w}{\tau_{wo}} = \frac{z}{e^z - 1} \qquad \text{where:} \quad z = \frac{2F}{C_{fo}}$$

This analysis is termed the "Couette flow model" (References 5 and 13) or alternatively "film theory" (Reference 14). Since St$\approx$C$_f$/2, the convective heat flux is decreased by the same factor. It is convenient to rearrange the expression to a logarithmic form, where the argument contains the actual Stanton number (St), rather than the unblown value (St$_o$). Substituting $\dot{Q}_{conv} = $ St G C$_{pg}$ ΔT, gives a simple result:

$$\frac{h}{h_o} = \frac{\ln(1+H)}{H} \qquad \text{where:} \quad H = \frac{F}{St} = \frac{C_{pg}}{\lambda}\left[\Delta T + \frac{\dot{Q}_{rad}}{h}\right]$$

8

Without radiation, the convective heat flux decrease depends only upon the non-dimensional factor $C_{pg}\Delta T/\lambda$, termed the "Spalding transfer number" in droplet evaporation research. With radiation, h must be determined implicitly.

Results of more sophisticated transpiration analyses are compared with the Couette flow model in Figure 3. Since the existing experimental data shows considerable scatter, there is no advantage in using the more complicated analyses.

To account for an injectant different than the free stream gas, the parameter H must be multiplied by a correction factor, K_M, being either the vapor to gas specific heat ratio to the power 0.6 (References 5 and 15) or the gas to vapor molecular weight ratio to the same power (Reference 16), when $M_c < M_g$. These two forms are identical for ideal gases with the same γ. For $M_c > M_g$, Rubesin (Reference 16) gives the exponent as 0.35. The data of References 5 and 15 was for $M_c < M_g$ only and thus does not contradict this second exponent. These corrections are confirmed by Landis' turbulent boundary layer model (Reference 3).

Since the specific heats were considered in the transpiration model, they should not require a separate accounting. However, a molecular weight difference would require a correction term, because a lower density injectant would displace a greater volume in the boundary layer, decreasing the heat flux. The effect should be less pronounced when the injectant has a greater density than the free stream gas, as given by Rubesin's second exponent. For this reason the correction term based upon the molecular weight ratio, as suggested by Rubesin, is used in the model as:

$$K_M = \left[\frac{Mg}{Mc}\right]^a \qquad \text{where:} \quad a = \begin{array}{ll} 0.60 & \text{for } M_c < M_g \\ 0.35 & \text{for } M_c > M_g \end{array}$$

2.1.3 Liquid Film Disturbances

Two types of disturbance to the surface of the liquid film have been observed. These have been studied by Kinney (Reference 17), Knuth (Reference 18), and Gater (Reference 19).

The first type of disturbance is the appearance of random, small-scale structures, with a pebbled appearance. These disturbances are always present and cause an effective surface roughness which may increase the heat flux. Photographic studies show that the length scales of these disturbances decrease at

higher velocities, although no general correlations were determined (References 17, 18).

The other type of disturbance, realized at higher coolant flow rates, is the appearance of large waves traveling in the flow direction. These waves exist only at the upstream positions where the liquid film is thick enough to sustain them. The mass loss rate in the regions where these waves do exist is 2 to 4 times the normal evaporation rate, independent of the film thickness. Shearing of droplets from the crests of the waves, without evaporation, is considered the primary mechanism of increased mass loss.

The point of onset of the large waves is well defined. Knuth was able to correlate both his data and that of Kinney for the transition point. Assuming that the mixture above the liquid film is mostly vapor and that the vapor to liquid viscosity ratio is greater than 0.03, Knuth's correlation for the critical liquid mass flow per circumference is:

$$\Gamma_{cr} = 1.01 \times 10^5 \ \mu_v^2/\mu_l$$

Gater found quite different results. In photographic studies he noticed large waves only for water coolant. Mass was lost without evaporation for all of his test conditions. Furthermore, the mass loss rate was dependant upon the local film thickness, proportionate to the local flow rate.

These differences might be explained by the different experimental arrangements. Kinney and Knuth both measured the length of the liquid film for different liquid flow rates by determining the dryout point, using axially spaced thermocouples. Gater used a fixed film length and captured the excess liquid in a downstream slot. Obviously the potential existed for some of the liquid to flow past the capture slot. At high injection rates it is also difficult to insure that all of the liquid is placed on the wall. Knuth considered this problem in detail. Either of these problems might explain the different results of Gater. In favorably comparing his proposed correlation with Kinney's data, Gater employed an adjustable constant and failed to properly account for quantities on a unit area basis.

Liquid film waves have also been studied with application to chemical processes. Hanratty and Hersham (Reference 20) give a correlation for the free stream velocity at the transition to large waves in terms of the gravitational constant. However, they were unable to explain the results of Kinney and Knuth in a horizontal tube. Apparently their correlation is useful only in vertical tubes at low gas velocities. Woodmansee and Hanratty (Reference 21) measured:

Γ_{cr} = 0.0641 kg/m-s for water, which is about 3 times lower than predicted by Knuth's correlation. Of related interest, Tatterson and Dallman (Reference 22) give a correlation for the mean diameter of the droplets sheared off of the liquid film.

The present model is valid only when the liquid flow rate is below the critical value given by Knuth's correlation. The small-scale disturbances are not assumed to increase the convective heat flux.

2.2 RADIATIVE HEAT TRANSFER

In most rocket combustion chambers the radiant heat flux is negligible in comparison with the convective heat flux (References 23 and 24). However, the transpiration of vapor from the liquid film decreases the normally expected convective flux to the extent that the radiant flux may become dominant in determining the liquid evaporation rate.

The radiation from combustion products is difficult to calculate from first principles due to the complicated molecular spectra of the many species present. Molecular band models attempt to replace the actual spectral lines present with a statistical distribution of lines, having the same gross properties. Such modeling is a major research effort and was not warranted in the present study. However, with access to spectral codes, it is preferred to the simple approach described here.

Fortunately, in a high temperature, high pressure environment many of the gas spectral properties can be more simply treated. High temperature causes each spectral line to be "doppler broadened" due to kinetic motion. Even more significant is "collision broadening", due to high pressure. This broadening tends to smear the spectrum lines together into continuous bands. With a large number of different species, there would be few gaps in the spectrum. Soot radiation aids in filling the gaps. In the limit, a very dense gas mixture in thermodynamic equilibrium radiates as a perfect blackbody.

2.2.1 Total Emittance of Gas

The total emittance of a gas is the ratio of the radiant intensity of the gas to that of a blackbody at the same temperature, averaged over the entire spectrum. This quantity is much easier to measure than the detailed spectral data and has been available for many years. Unfortunately data is available only for H_2O and CO_2, however, this covers many cases of combustion interest since symmetric diatomic

molecules, such as N_2, do not radiate significantly.

The most recent emittance data at 1 atm pressure is compiled by Siegel and Howell (Reference 25). This data is replotted in Figure 4 as a function of the optical density, ρ_{opt}, which is the gas partial pressure times the path length through the gas. Note that at very high optical densities the emittances reach limiting values, ϵ_f, of 0.825 for H_2O and 0.231 for CO_2. These curves may be analytically fit to a function:

$$\epsilon = \epsilon_f \left[1 + \left[\frac{\rho_{opt}}{c}\right]^{-n} \right]^{-1/n}$$

with coefficients:

T (°K)	H_2O c(atm·m)	n	T (°K)	CO_2 c(atm·m)	n
1000	0.165	0.45	1000	0.05	0.6
2000	0.90	0.65	1500	0.075	0.6
3000	2.05	0.61	2000	0.15	0.6

A three point interpolation is used for temperatures between these.

A correction is required for pressures other than 1 atm by multiplying a correction factor, K_p, to each emittance. The curves for these pressure corrections are fit by the functions:

H_2O: $K_p = 1 + C_1 \{1-\exp[(1-P[1+N_w])/C_2]\}$

where: $C_1 = 0.26 + 0.74 \exp(-2.5\ \rho_{H_2O})$
          $C_2 = 0.75 + 0.31 \exp(-10\ \rho_{H_2O})$ atm

CO_2: $\log_{10} K_p = 0.036\ \rho_{CO_2}^{-0.483}[1+(2\ \log_{10}P)^{-m}]^{-1/m}$

where: $m = 100\ \rho_{CO_2}$

An additional correction is necessary to account for overlaps in the two spectra. This correction (for T > 1200K) is fit by:

$$\Delta\epsilon = 0.0551\ K_x\ [1-\exp(-4\ \rho_{opt})]\ [1-\exp(-12.5\ \rho_{opt})]$$

where: $K_x = 1 - \left| \frac{2\ N_w}{N_w + N_c} - 1 \right|^n$

          $n = 5.5\ [1+(1.09\ \rho_{opt})^{-3.88}]^{-1/3.88}$

In the equations above:

$$P_{H_2O} , P_{CO_2} , P_{opt} <> atm \cdot m$$
$$P <> atm$$
$$N_w = \text{mole fraction of water in mixture}$$
$$N_c = \text{mole fraction of } CO_2 \text{ in mixture}$$

The total gas emittance is then:

$$\epsilon_g = \epsilon_{H_2O} + \epsilon_{CO_2} - \Delta\epsilon$$

To evaluate these terms it is necessary to input the optical path length through the gas. Since this generally varies over the sight angle, the most direct method would be to calculate the emittance at a number of sight angles and to average them, weighted by the projected area at each angle. However, a simpler approach is to use an overall effective length. A very simple expression is quite accurate in determining the effective length (Reference 25): $L_{eff} = 0.95(4V/A)$, where V is the chamber volume and A is the surrounding surface area.

In applying this formula, the downstream section of the chamber can be assumed to be an infinite cylinder, for which $L_{eff} = 0.95 D$. If the cloud of droplets coming out of the injector is assumed to be perfectly reflective, then the upstream direction can also be considered an infinite cylinder. Since the droplets have numerous partially reflecting surfaces this is probably the best assumption.

Alternatively, if the droplets are assumed to be perfectly absorbing then the effective upstream length is: $L_{eff} = 0.95D[4x/(D+4x)]$. The upstream and downstream emittances are then averaged to obtain the total emittance. With this assumption the radiant heat flux must be calculated at every axial position.

It is also necessary to consider the possibility of reflective walls. Reflective walls increase the effective sight paths. The simplest correction, due to Egleti (Reference 26), is to multiply the effective length above by a factor A_w to the power -0.85 ; where A_w is the wall absorptivity.

With the gas emittance determined, the radiant heat flux is calculated as:

$$\dot{Q}_{rad} = \sigma A_w \epsilon_g [T_g^4 - T_v^4]$$

where: $\sigma = 5.67 \ 10^{-8} \ W/m^2 \cdot °K^4$

A final concern is that the above relations are for the radiation from hot gases in chemical equilibrium. However, there is evidence that the radiation from transient species can be important. Ziebland (Reference 26) measured an emittance of 0.22 in a small O_2/H_2 rocket operating at 10 atm. The radiation peak, which occurred at a position 8 cm from the injector face, was almost three times the expected value. Some 20 cm downstream, the emittance settled to the expected value. This initially large radiation was attributed to radiation by transient OH. While the radiation from OH in atmospheric flames contributes only a faint blue glow of no significant intensity, at high pressures it becomes significant (Reference 27). Since OH concentrations are difficult to calculate, radiation by OH was not considered in the present model.

2.2.2 Liquid Film Burnout

The radiant heat can penetrate the liquid film and be absorbed directly at the combustion chamber walls. It is then conducted into the liquid film by boiling heat transfer. With a high enough heat flux the liquid film can "burnout", as in normal pool boiling.

The same geometry of a thin liquid film flowing across a heated surface has been studied by Monde and Katto (Reference 28), Katto and Ishii (Reference 29), and Mudawwar, et. al. (Reference 30). They all correlated the burnout heat flux as:

$$\frac{\dot{Q}_{bo}}{\rho_V \lambda U} = C \left[\frac{\rho_\ell}{\rho_V}\right]^{n_1} \left[\frac{\sigma}{\rho_\ell L U^2}\right]^{n_2}$$

where ρ_V and ρ_ℓ are the densities of the vapor and liquid, σ is the surface tension, λ is the latent heat of vaporization, L is the length of the heated surface, and U is the average velocity of the liquid film.

The constants fit to the data by each group and the parameter ranges are given below:

Group	C	n_1	n_2	U(m/s)	L(cm)
Monde and Katto	0.0591	0.725	0.333	3 to 26	0.56, 1
Katto and Ishii	0.0164	0.867	0.333	1.5 to 15	1 – 2
Mudawwar, et.al.	0.0881	0.867	0.432	0.4 to 2	6.4, 12.7

Monde and Katto studied a circular jet of water and Freon®113 impinging downward on a heated plate. Katto and Ishii studied a plane jet of water,

Freon® 113, and 1,1,1-trichloroethane flowing across a heated plate. Mudawwar, et. al. studied a film of Fluorinert® liquid (FC-72) flowing downward along a heated surface. Since they used a single liquid, they assumed the same density ratio exponent, n_1, as Katto and Ishii. Since Katto and Ishii's test conditions appear to be closer to those for liquid film cooling in rocket engines, their correlation is used.

All of the researchers observed that when the critical heat flux was exceeded, the liquid film separated from the heated surface. Katto and Ishii observed that with water, the separation occurred upon first contact with the heated surface, whereas the organics maintained contact with the surface for some distance before separating. Mudawwar, et. al. observed separation upon first contact with the surface for their Fluorinert® tests. They also observed that the film reattached to the surface when the surface temperature was decreased.

This total separation of the film from the surface in the experiments may have been due to the constant heat flux condition imposed. In a rocket engine the liquid film would be less susceptible to burnout than in these heat transfer experiments because separation of the liquid film from the surface would generate a region of droplets and bubbles which would cause scattering, decreasing the radiative transmission through the film.

Use of these burnout correlations is questionable since they are expressed in terms of the overall heated length. Ideally, the burnout point should be expressed in terms of local conditions, such as the local film thickness. They are mainly useful as an order of magnitude calculation. With this in mind, the burnout heat flux for several rocket fuels is calculated below for the case: L = 5 cm and U = 1.5 m/s, at a pressure of 100 psia (data Reference 31):

Fuel	Tsat ($^\circ$K)	λ (10^3J/kg)	ρ_l (kg/m^3)	ρ_v (kg/m^3)	σ_l (10^{-3}N/m)	$\dot{Q}_{bo}$ (kW/m^2)
MMH	433	663	720	9.79	20.2	419
Az50	413	870	778	9.50	18.	548
H$_2$	29	335	70	5.75	0.6	17.6

In most rocket engines the radiant flux slightly exceeds these critical values. However, some of the radiant heat is absorbed by the liquid film. Since hydrogen has such a low predicted burnout heat flux and does not absorb infrared radiation, it appears unsuitable for liquid film cooling.

Katto et. al. suggest a correction factor when the liquid is injected at a temperature below the saturation temperature, however it was not correlated over a

large range and is significantly larger than such correction factors for pool boiling. If the burnout point is controlled only by local conditions, and the liquid is heated to the saturation temperature at the burnout point, then no sub-cooling correction should be necessary, therefore none is used in the present model.

The fraction of radiation transmitted through the liquid film is: $\exp(-\alpha t)$; where α is the absorptivity of the liquid, averaged over the spectrum of the radiation. The liquid film thickness, t, is calculated from the wall shear stress. Assuming laminar flow:

$$t = \left[\frac{2\ \mu\ \Gamma}{\rho\ \tau_w}\right]^{\frac{1}{2}}$$

where Γ is the local coolant mass flow per circumference. The surface shear stress, τ_w, is calculated by Equation 2.1, with the transpiration correction of Section 2.1.2 . For simplicity h/h_o is used in place of τ_w/τ_{wo}.

The average liquid film velocity, needed for the correlation, is: $U = \Gamma/(\rho t)$. The surface velocity of the liquid, needed in Section 2.1, is twice this average film velocity.

Using these values, the burnout heat flux is calculated with Katto and Ishii's correlation at each axial position in the rocket chamber and compared with the radiant heat flux transmitted through the liquid film. A warning results when the radiant flux exceeds the burnout heat flux. However, as discussed in Section 4.0, this burnout warning was not found to give a reasonable comparison with any of the data analyzed.

2.3 COMPARISON WITH OTHER ANALYSES

2.3.1 Purdue University Jet Propulsion Center (JPC):

A number of liquid film cooling analyses have been presented by researchers from the Jet Propulsion Center at Purdue. In early studies Zucrow and Graham (Reference 32) attributed the increased mass loss rate after transition not to large surface waves, but to variations in the termination point of the liquid film around the circumference. Zucrow and Sellers (Reference 33) attempted to model the mass transfer with no real success.

In a later analysis Warner and Emmons (Reference 34) gave a result which was restated by Ziebland (Reference 26). For the no blowing case it reduces to an unusual result:

$$St = \frac{1}{2} C_f \mu (PrU_g)^{-1}$$

It was not possible to reproduce their calculations with the suggested constants, even after correcting for an apparent sign error in their Equation 5, so their analysis was not considered further.

Gater, et. al. (Reference 35) attempted to relate all of the previous expressions from the JPC. In a later report (Reference 19), Gater mentions the transpiration analysis of Section 2.1.2, but discounts it due to the anomalies in his data mentioned in Section 2.1.3 .

2.3.2 Shembharkar and Pai (Reference 36)

These authors use a Prandtl mixing length turbulence model for the gas convection, coupled to a viscous flow model for the liquid film. Landis (Reference 3) and Economis (Reference 37) reported similar turbulent boundary layer models which gave no real improvement over the simple Couette flow transpiration model, so the need for this complexity is questionable.

In their datum case, the starting boundary layer thickness is 12.5 mm, corresponding to a downstream starting position of $x = 0.812$ m, by the boundary layer growth relations of Section 3.0 . Since the boundary layer is well developed upon contacting the relatively short liquid film, the evaporation rate should be almost constant. Instead, they calculate an initially high evaporation rate of 0.2 kg/s-m^2, dropping exponentially to 0.124 kg/s-m^2, possibly due to numerical problems. The simpler analysis of the present report predicts an almost constant evaporation rate of 0.106 kg/s-m^2. The difference between this and their final evaporation rate is exactly accounted for by the blowing correction factor (h/ho). It is not apparent that the momentum of the transpiring vapor was properly included as a boundary condition in their model. This vapor momentum is what causes the convective heat flux decrease in transpiration cooling.

2.4 SUMMARY OF LIQUID FILM EVAPORATION ANALYSIS

This section summarizes the equations and calculation order used in the liquid film evaporation model. A simple algebraic formulation is given first, suitable when radiation is negligible and the flow is either fully-developed or purely boundary layer.

2.4.1 Simple Expression

Without radiation, the liquid film length, L_C, is determined from the coolant flow (per circumference), Γ, and the convective evaporation rate, $\dot{m}_{conv}$, as:

$$L_C = \Gamma/\dot{m}_{conv}$$

Substituting Equation 2.4, with the transpiration correction,

$$L_c = \frac{\Gamma \; \lambda^*}{GC_{pg}\Delta T \; St_o(h/ho)}$$

For fully developed flow ($L_C > 5D$), St_o is constant and is calculated with Equation 2.3, allowing L_C to be calculated above.

For pure boundary layer flow ($L_C < 2D$), with liquid injection at $x=0$, the average Stanton number is 1.25 times higher than that at $x=L_C$ (found by integrating Equation 2.2 from $x=0$ to $x=L_C$). Thus:

$$St_o|_{avg} = 1.25[0.0296(GL_C/\mu_g)^{-0.2}Pr^{-0.6}]$$

Substituting above:

$$L_c = \frac{61.62 \; \mu}{G} \left[\frac{\lambda^* \; \Gamma}{C_{pg} \; \Delta T \; \mu_g(h/ho)} \right]^{1.25} Pr^{0.75}$$

Without radiation, the transpiration correction of Section 2.1.2 reduces to a simple form:

$$h/ho = \frac{\ln(1+H)}{H} \qquad \text{where:} \qquad H = \frac{C_{pg} \; \Delta T}{\lambda^*} K_M$$

2.4.2 Complete Formulation

The equations used in the liquid film evaporation FORTRAN program "liquid.for" are summarized below.

The radiant emittance of the hot combustion products is calculated first in subroutine "Emittance" as:

$$E_g = \text{Emittance}(P, L_{eff}, T_g, N_w, N_c)$$

where: $L_{eff} = 0.95 \, D \, A_w^{-0.85}$

giving: $\dot{Q}_{rad} = \sigma \, A_w \, \epsilon_g \, [T_g^4 - T_v^4]$

Subroutine "Emittance" is a direct coding of the curve fits of Section 2.2.1. Parabolic interpolation is used between the three temperature curves for CO_2 and H_2O in function "Fit". Since a constant L_{eff} is assumed (i.e. reflective droplets), the radiative heat flux is constant, independent of axial position.

Axial steps:

Beginning at the liquid film injection point, the local convective coefficient without transpiration is calculated as:

$$h_o = K_t G \, C_{pg} St_o$$

where: $K_t = 1 + 4e_t$ "turbulence correction factor"
$St_o = \tfrac{1}{2} C_f Pr^{-0.6}$
$C_f = 0.0592 \, Re_x^{-0.2}$
$Re_x = G \, x_e / \mu_g$
$G = G_{ch}(T_g/T_m) [(U_g - U_1)/U_g]$
$x_e = 3.53D\{1 + [x/(3.53D)]^{-1.2}\}^{0.8333}$
$T_m = \tfrac{1}{2}(T_g + T_v)$

The convective heat flux with transpiration is calculated implicitly as:

$$h = h_o \ln(1+H)/H$$

where: $H = C_{pg} \, K_M \, \dot{m}_{vap} / h$

$K_M = (M_g/M_v)^a$; $a=0.6$ if $M_v < M_g$
                               $a=0.35$ if $M_v > M_g$

19

$\dot{m}_{vap}$ is the liquid evaporation rate per surface area, calculated below. The wall shear stress is decreased by this same factor, so that:

$$\tau_w = \tau_{wo}(h/h_o)$$

$$\text{where:} \quad \tau_w = \tfrac{1}{2}C_f G(U_g-U_l)$$

The convective heat flux is then: $\dot{Q}_{conv} = h\,\Delta T.$

The initial temperature rise of the liquid film is:

$$dT_{liq}/dx = \dot{Q}_{tot}/(\Gamma C_p) \quad \text{for} \quad T_{liq}<T_v$$
$$\text{where:} \quad \dot{Q}_{tot}=\dot{Q}_{conv}+\dot{Q}_{rad}$$

Once $T_{liq}=T_v$, the liquid evaporates at a rate (per area):

$$\dot{m}_{vap} = \dot{Q}_{tot}/\lambda$$

which decreases the liquid flow per circumference at a rate $d\Gamma/dx = -\dot{m}_{vap}$. The position at which $\Gamma = 0$ is the "film-cooled length", L_c.

The liquid film thickness and average velocity are calculated using the simple laminar "Couette flow" result:

$$t = \text{sqrt}[2\mu\Gamma/(\rho\tau_w)]$$
$$U_{liq} = \Gamma/(\rho t)$$

The surface velocity of the liquid is twice this average velocity: $U_l=2U_{liq}$

The possibility of liquid film burnout is tested. The burnout heat flux limit is calculated as:

$$\dot{Q}_{bo} = 0.0164\lambda\rho_l{}^{0.534}\rho_v{}^{0.133}(U_{liq}\sigma/x_{liq})^{0.333}$$

This is compared with the radiant heat transmitted to the wall:

$$\dot{Q}_w = \dot{Q}_{rad}\exp(-\alpha t)$$

When $\dot{Q}_w > \dot{Q}_{bo}$, a warning is printed in the output file. However, this warning has been found unreliable.

20

3.0 GASEOUS FILM COOLING

After the liquid film has vaporized it continues to provide thermal protection
to the wall by calorimetric mixing with the hot free stream gas entrained in the
boundary layer. Numerous correlations have been presented for this process,
termed "gaseous film cooling". They are normally expressed in terms of a "cooling
effectiveness":

$$\eta = \frac{Tg - Taw}{Tg - Tc}$$

where T_g is the free stream gas temperature, T_c is the initial coolant temperature,
and T_{aw} is the "adiabatic wall" temperature in the boundary layer which results
from calorimetric mixing of the two gas flows. The cooling effectiveness is a
function of a non-dimensional distance (X) downstream of the injection point:

$$X = K \ x$$

where: $K = G \ \mu_g^{\ 0.25} \ \dot{M}_c^{\ -1.25}$

$\dot{M}_c$ = coolant mass flow per circumference
$G = \rho_g U_g$ = free stream mass flow
x = downstream distance

Most authors arrange the constant K in terms of a coolant Reynolds number,
giving the false impression that the injection velocity is important. As long as the
coolant is injected with low relative velocity so that there are no jet effects, the exact
geometry of the injection point is unimportant.

The most successful analysis is that of Kutateladze, et al (Reference 38) and
Stollery, et al (Reference 39, Equation 27) for gaseous film cooling on a flat plate in
turbulent flow, with coolant injection at the leading edge. To specify the conditions
of the boundary layer downstream of the injection point, they conceptually replace
the injected coolant with an equivalent mass of free stream gas. To provide the
proper boundary layer growth rate, they identify an effective leading edge a distance
x_0 upstream of the true leading edge (at $x=0$). Their analysis can be extended to
the case of injection at a point x_i downstream of the true leading edge as follows,
with the nomenclature defined in Figure 5.

From the solution to the boundary layer integral equations for a $1/7^{th}$ power
law velocity profile (Reference 2), the boundary layer thickness and mass flow (per
width) a distance x' from the effective leading edge is:

$$\delta = 0.371x'Rex'^{-0.2} \qquad \text{where: } x' \equiv x+x_0$$

$$\dot{M}_{bl} = 7/8 \ G\delta = 0.325\dot{M}_c[X+X_0]^{0.8} \qquad \text{(Equation 3.1)}$$

The fictitious upstream point X_0 is found from a mass balance at the injection point:

$$\dot{M}_{bl}|_{x=xi} = \dot{M}_c + \dot{M}_{up}$$

$$0.325 \ \dot{M}_c(X_i+X_0)^{0.8} = \dot{M}_c + 0.325 \ \dot{M}_cX_i^{0.8} \qquad \text{(Equation 3.2)}$$

Thus,

$$X_0 = (3.08+X_i^{0.8})^{1.25}- X_i$$

$$\text{where: } \quad X_i = K \ x_i$$

The total mass of free stream gas entrained up to position x is:

$$\dot{M}_g = \dot{M}_{bl} - \dot{M}_c \qquad \text{(Equation 3.3)}$$

From a calorimetric heat balance:

$$\eta = \left[1 + \frac{Cpg}{Cpc} \frac{\dot{M}_g}{\dot{M}_c}\right]^{-1} = \left[1 + \frac{Cpg}{Cpc}\left(\frac{\dot{M}_{bl}}{\dot{M}_c}-1\right)\right]^{-1}$$

giving,

$$\eta = \left[1 + \frac{Cpg}{Cpc}(0.325[X+X_0]^{0.8} - 1)\right]^{-1} \qquad \text{(Equation 3.4)}$$

Other correlations based upon similar analyses have been proposed (Reference 39, 40, 41). However, most of these are less careful about accounting for the effects of the injectant upon the boundary layer growth downstream of the injection point. At large downstream distances most reduce to the same form. The correlation above gives excellent comparison with most experimental data (Reference 39, 42).

This analysis can be extended to the case of distributed injection, as exists in the liquid film cooling process, with the vapor injected continuously along the liquid film length. However the resulting expression is unwieldy. In any event, the exact injection point is of minor concern. Librizzi and Cresci's analysis (Reference 41), which gives predictions very close to Equation 3.4, does not even require the position of coolant injection.

This analysis contains two assumptions which are known to be wrong. These are that all of the gaseous coolant remains in the boundary layer and that all of the gases in the boundary layer are at the same temperature, T_{aw}. In fact, measurements of the concentration and temperature profiles show an S-shaped

profile for both (Reference 43). However, these profiles do maintain a similar shape, growing away from the wall at the same rate as the boundary layer thickness. This suggests that the above analysis can be reinterpreted.

The S-shaped temperature profile can be conceptually divided into a two domain region, an outer layer at the free stream temperature and an inner layer at T_{aw}. Since this inner layer thickness is a constant fraction of the total boundary layer thickness, the same mass ratio of hot gases will be entrained as in the original analysis, giving the same cooling effectiveness. However, in this case the interpretation is that T_{aw} is the temperature only in the region very close to the wall.

Even with this re-interpretation a difficulty remains, in that the analysis predicts no free stream gas entrainment in fully-developed flow, which is certainly unrealistic for turbulent flow. Indeed, Equation 3.4 is used in Section 4.2 for fully-developed flows, with satisfactory results. That the analysis leading to Equation 3.4 is apparently flawed should not detract from the fortuitous result that it correlates all existing data well.

A number of corrections to Equation 3.4 are necessary to account for effects not considered in the standard flat-plate boundary layer analysis. Corrections for free stream turbulence, foreign gas injection, thermal radiation, and changing free stream conditions are considered below.

3.1 FREE STREAM TURBULENCE

The flat-plate boundary layer relations used in deriving Equation 3.4 assume no free stream turbulence. Two experimental studies measured the effects of turbulence upon gaseous film cooling (References 44 and 45). A possible correction to the above analysis is to multiply the non-dimensional distance X by a factor $K_t = 1 + C_t$. This allows the increased mixing caused by the free stream turbulence to be accounted for as an effectively larger downstream distance. When applied to the data of Marek and Tacina (Reference 44), C_t is found to be constant with X and varies with the free stream turbulence rms fraction, e_t, as: $C_t = 8.67 \, e_t$, for $e_t = 0.07$, 0.14, and 0.23. For $e_t = 0.35$, the data follows this relation for $X < 1.5$, thereafter C_t increases as $X^{0.3}$.

Unlike Marek and Tacina, Carlson and Talmor (Reference 45) did not directly measure the turbulence level, but inferred it based on screens placed in the flow. The length scales of their turbulence may also have differed considerably

from Marek and Tacina's. Analyzing their data gives: $C_t = 11.7\,e_t$. In their data C_t varied slightly with X at all turbulence levels. The expression above is an average over X. Since their greatest turbulence level was 22%, the increased mixing found by Marek and Tacina at 35% turbulence was not confirmed. For the present model the two results were averaged, giving a correction term:

$$K_t = 1 + 10.2\,e_t$$

3.2 FOREIGN GAS INJECTION

Goldstein, et. al. (Reference 43) found that the effectiveness values were about 30% higher than expected when helium replaced air as the coolant injected into a heated airstream. These results were confirmed by Burns and Stollery (Reference 46). However, Carlson and Talmor (Reference 45) questioned whether the effect should be attributed to the coolant properties, since the helium injection velocities were lower than the air injection velocities at the same effectiveness values.

In the present model the effect is assumed to be real and is attributed to the molecular weight difference, for the same reasons stated in Section 2.1.2 . Goldstein fit his data with an empirical equation (Reference 43, Equation 12). Apparently he failed to recognize that this empirical equation could be put into the form of Equation 3.4 by multiplying a correction factor, K_M, of 0.76 to the (Cpg/Cpc) ratio. Assuming a power function dependance of this correction factor upon the molecular weight ratio, and generalizing from this specific case of a coolant to gas molecular weight ratio of 0.138, the correction factor can be written in general as:

$$K_M = (Mc/Mg)^{0.14}$$

With these corrections for turbulence and foreign gas injection, Equation 3.4 becomes:

$$\eta = \left[1 + K_M\left[\frac{Cpg}{Cpc}\right]\left[0.325(K_t X + Xo)^{0.8} - 1\right]\right]^{-1} \qquad \text{(Equation 3.5)}$$

3.3 THERMAL RADIATION

The radiant heat flux is transmitted through the boundary layer and absorbed at the wall. This heat is then conducted back into the boundary layer gases, requiring a wall temperature, T_w, in excess of the boundary layer temperature, T_{aw}:

$$T_w = T_{aw} + \dot{Q}_{rad}/h$$

This form is suggested for gaseous film cooling with a non-adiabatic wall (Reference 47). The heat transfer coefficient is calculated by Equation 2.2, evaluated at $x' = x + x_0$.

The radiant heat also enters into the heat balance of the boundary layer gases. Assuming that it is spread evenly over the entire boundary layer mass, the rate of temperature increase with distance is:

$$\frac{\Delta T_{aw}}{\Delta x} = \frac{\dot{Q}_{rad}}{M_{bl} C_{pg}}$$

3.4 NON-UNIFORM FREE STREAM FLOW

Equation 3.5 was derived for a constant free stream gas flow rate and temperature. If these quantities change as the flow proceeds downstream, then Equation 3.5 cannot be directly applied. To demonstrate this, consider a sudden decrease in the flow rate per area, G. Applying Equation 3.5 locally would imply a sudden decrease in the non-dimensional distance, X, and a step increase in the effectiveness, η. This would suggest that the gases spontaneously unmix, violating the second law of thermodynamics.

Due to the parabolic nature of the boundary layer equations, the local conditions determine only the rate of change, in the downstream direction, of the boundary layer properties. Equation 3.5 is an integral result for the special case of constant flow conditions. However, it can easily be rearranged in the form of a differential equation.

The rate of change of η with position x is determined by differentiating Equation 3.5 . All parameters are held constant in differentiating, since such was assumed in deriving the integral expression. Expressing the result in terms of the local value of η:

$$d\eta/dx = -0.1963 \; K \; K_t K_M \left[\frac{Cpg}{Cpc}\right]\eta^2 \left[1 + \frac{Cpc}{K_M Cpg}\left[\frac{1}{\eta} -1\right]\right]^{-\frac{1}{4}}$$

η is found by numerically integrating this expression. The initial condition on η at the injection point could be found from Equation 3.5. However, this predicts $\eta < 1$ at the injection point when injection is downstream of the leading edge, which is unsupported. A more realistic assumption that $\eta = 1$ at the injection point is used as the initial condition in the present study. The above approach is termed the "differential η" formulation to distinguish it from the "integral correlation" of Equation 3.5 .

The free stream mass flow rate per area, G, varies inversely with the local cross-sectional area as:

$$G = G_{ch}(A_{ch}/A)$$

Increases in G, as the nozzle converges, increases the rate of free stream gas entrainment through the coefficient K.

The other effect of free stream acceleration is a drop in the static temperature of the free stream gas. Upon entrainment into the boundary layer the original stagnation temperature is recovered as the kinetic energy is converted back into thermal energy. However, some of this heat is then lost by conduction back into the cooler free stream gas. The result is that the free stream gas attains a temperature in the boundary layer lower than the stagnation temperature. This is termed the "recovery temperature", T_r, and is normally a constant fraction of the difference between the static and stagnation temperatures:

$$T_r = T_0-(1-r)(T_0-T_s)$$

where T_0 and T_s are the static and stagnation temperatures of free stream gas and r is the "recovery factor".

This recovery temperature should replace T_g in the equations above. For a flat-plate boundary layer without gaseous film cooling, $r = Pr^{1/3}$ (Reference 48). It is assumed that this relation holds for the gaseous film cooling case, although this assumption is questionable.

From the isentropic relations for compressible flow:

$$T_s = T_0/[1+ \frac{1}{2}(\gamma-1)M^2]$$

26

The local Mach number, M, is found implicitly from one of two forms:

$$M = \frac{1}{A_t} \left[\frac{2}{\gamma+1} + \frac{M^2}{\gamma_r} \right]^{\gamma_r/2} \qquad \text{for} \quad M<1$$

or

$$M = \left[\gamma_r (MA_t)^{2/\gamma_r} - \frac{2}{\gamma-1} \right]^{\frac{1}{2}} \qquad \text{for} \quad M>1$$

where: $\quad A_t \equiv (A/A_{throat})$

$$\gamma_r = \frac{\gamma+1}{\gamma-1}$$

3.4.1 Differential Entrainment Formulation

When the recovery temperature changes, the "differential η" formulation becomes invalid, for the subtle reason that the local value of η no longer determines the local state of the boundary layer. This problem is remedied by recognizing that the true local state of the boundary layer is determined by the local mass flow rate in the boundary layer, $\dot{M}_{bl}$. From Equation 3.1, the local entrainment rate is:

$$\left. \frac{d\dot{M}_{bl}}{dx} \right|_e = 0.1963 \ G \left[\frac{\mu_g}{\dot{M}_{bl}} \right]^{-0.25} \qquad \text{(Equation 3.6)}$$

The calorimetric heat balance in differential form is:

$$d\dot{M}_{bl} C_{pg} (T_r - T_{aw}) = (\dot{M}_g C_{pg} + \dot{M}_c C_{pc}) dT_{aw}$$

The specific heat on the left side should be evaluated at the mean temperature of T_r and T_{aw}, while those on the right should be evaluated at T_{aw}. Substituting Equation 3.3, and dividing both sides by dx:

$$\frac{dT_{aw}}{dx} = \left. \frac{d\dot{M}_{bl}}{dx} \right|_e (T_r - T_{aw}) \left[\dot{M}_{bl} + \left[\frac{C_{pc}}{C_{pg}} - 1 \right] \dot{M}_c \right]^{-1} \qquad \text{(Equation 3.7)}$$

To apply these relations, Equations 3.6 and 3.7 are integrated to determine $\dot{M}_{bl}$ and T_{aw} at each x position. As stated, T_{aw} is equated to T_c (or $\eta = 1$) at x = 0. The initial condition on $\dot{M}_{bl}$ is found from Equation 3.2:

$$\left. \dot{M}_{bl} \right|_{xi} = \dot{M}_c [1 + 0.325 X_i^{0.8}]$$

In applying this to the curved walls of a rocket chamber, x is measured along the contour of the nozzle.

This "differential entrainment" formulation is the most general. Although the derivation is more involved, it requires no more computation than the previous "differential η" formulation. For the case of constant free stream gas temperature, where the local value of η is directly related to M_{bl}, both formulations are equivalent. And, of course, for constant free stream conditions, both reduce to the integral correlation (Equation 3.5).

To include the effects of free stream turbulence and foreign gas injection, the coefficient in Equation 3.6 is multiplied by the factor K_t, and the (C_{pc}/C_{pg}) ratio in Equation 3.7 is multiplied by $1/K_M$. Both corrections are consistent with the placement of these factors in the differential η formulation.

3.4.2 Circumferential Change:

In a rocket engine the contraction of the nozzle decreases the circumference, causing an increase in the boundary layer mass flow per circumference:

$$\left. \frac{d\dot{M}_{bl}}{dx} \right|_c = - \dot{M}_{bl} \frac{1}{D} \frac{dD}{dx}$$

Since this increase is not due to free stream entrainment, it does not enter into the energy balance. However, it is important in that it affects the total boundary layer flow rate, which is found by adding the changes due to free stream entrainment and this circumferential change. This total boundary layer flow rate determines the local rate of free stream gas entrainment, as given by Equation 3.6. In adding this term to the analysis, the coolant flow rate per circumference should also be calculated locally, by scaling the chamber value.

3.5 TURNING EFFECTS

Carlson and Talmor (Reference 45) measured the effectiveness downstream of a sharp turn in a rectangular duct. Their results can be fit as:

$$\eta = [1 + CX^n]^{-1}$$

with coefficients:

turning angle	C	n
30°	0.40	2.2
45°	0.75	2.1
60°	1.40	2.0

To reduce approximately to Equation 3.4 the exponent, n, should approach 0.8 as the turning angle approaches 0°. Since the exponent is increasing in the opposite direction their results are somewhat anomalous. For unturned flows in a circular duct their results followed Equation 3.4. Possibly these results were due to disturbance of the boundary layer by the sharp turn in their wind tunnel.

Ewen and Rousar (References 49-51) studied gaseous film cooling in converging nozzles. Their data is analyzed in Section 4.0 and leads to a correlation for an increased entrainment in terms of a "centrifugal parameter".

3.6 CHAMBER CONTOUR

In general the shape of most rocket combustion chambers can be expressed in terms of a few parameters: l_1, r_1, θ_c, D_t, r_2, and θ_d, as shown in Figure 6. Given these, the limits of each segment are expressed:

$$l_2 = l_1 + r_1 \sin\theta_c$$
$$D_2 = D_{ch} - 2 r_1 (1-\cos\theta_c)$$
$$D_3 = D_t + 2 r_2 (1-\cos\theta_c)$$
$$l_3 = l_2 + (D_2-D_3)/(2\tan\theta_c)$$
$$l_t = l_3 + r_2 \sin\theta_c$$
$$l_5 = l_t + r_2 \sin\theta_d$$
$$D_5 = D_t + 2 r_2 (1-\cos\theta_d)$$

The chamber diameter is then calculated at any axial position, l, by:

$$\text{For:} \quad l_1 < l < l_2 \qquad D = D_{ch} - 2(r_1 - \text{sqrt}[r_1^2 - (1-l_1)^2])$$
$$l_2 < l < l_3 \qquad D = D_2 - 2(1-l_2)\tan\theta_c$$
$$l_3 < l < l_5 \qquad D = D_t + 2(r_2 - \text{sqrt}[r_2^2 - (1-l_5)^2])$$
$$l_5 < l \qquad D = D_5 + 2(1-l_5)\tan\theta_d$$

The downstream position along the wall, x, is related to the axial position, l, as:

$$(\Delta x)^2 = (\Delta l)^2 + (\Delta D/2)^2$$

This expression is integrated as axial steps Δl are made, to determine the contour length.

3.7 SUMMARY OF GASEOUS FILM COOLING ANALYSIS

This section summarizes the equations and calculation order used in the gaseous film cooling FORTRAN computer program "gas.for". A simple formulation is given first, suitable when the free-stream mass flow and temperature are constant and radiation is negligible.

Simple Expression:

With constant free stream conditions, the wall temperature is easily calculated from Equation 3.5:

$$T_{aw} = T_r - \eta \, (T_r - T_c)$$

where:

$$\eta = \left[1 + K_M \left(\frac{Cpg}{Cpc} \right) \left[0.325 (K_t X + Xo)^{0.8} - 1 \right] \right]^{-1}$$

$$X = K \, x$$

$$K = G \, \mu_g^{0.25} \, \dot{M}_c^{-1.25}$$

Complete Formulation:

Starting at the end of the liquid film, steps dx along the wall contour are made. The increase in boundary layer flow due to free stream entrainment is:

$$\dot{dM}_1 = 0.1963 K_t G (\mu_g / \dot{M}_{bl}|_i)^{-0.25} \, dx$$

where the turbulence correction $K_t = 1 + 10.2 e_t$. The new boundary layer flow is projected as: $\dot{M}_{bl}|_{i+1} = \dot{M}_{bl}|_i + \dot{dM}_1$. Following the 2nd order Runge-Kutta method, the change is recalculated ($\dot{dM}_2$) using $\dot{M}_{bl}|_{i+1}$. The average of the two is used:

$$\dot{dM}_e = \tfrac{1}{2} (\dot{dM}_1 + \dot{dM}_2)$$

The increase in boundary layer flow (per circumference) due to chamber contraction is:

$$\dot{dM}_c = - \dot{M}_{bl} (1/D) (dD/dx) \, dx$$

where dD/dx is the rate of change of diameter with contour length x, as expressed in Section 3.6.

The boundary layer flow at the next axial step is then:

$$\dot{M}_{bl}|_{i+1} = \dot{M}_{bl}|_i + (d\dot{M}_e + d\dot{M}_c)$$

The increase in boundary layer temperature due to the free stream mass entrainment is:

$$dT_e = d\dot{M}_e \ (T_r - T_{aw}) \left[\dot{M}_{bl} + \dot{M}_c \left[\frac{1}{R_M} \frac{c_{pc}}{c_{pg}} - 1\right]\right]^{-1}$$

The increase in boundary layer temperature due to thermal radiation is:

$$dT_{rad} = [Q_{rad}/(C_{pg}\dot{M}_{bl})]dx$$

The boundary layer temperature at the next step is then:

$$dT_{aw}|_{i+1} = dT_{aw}|_i + (dT_e + dT_{rad})$$

The wall temperature is higher than the boundary layer gas as:

$$T_w = T_{aw} + \dot{Q}_{rad}/h$$

where h is the convective heat transfer coefficient, as determined in Section 2.1 .

The recovery temperature (T_r) is determined by the local area ratio, as discussed in Section 3.4 . The local area ratio is determined by the contour equations of Section 3.6 .

4.0 COMPARISON WITH EXPERIMENTS

4.1 LIQUID FILM EVAPORATION

4.1.1 G.R. Kinney et al air-water experiment (Reference 17)

These heat transfer measurements were performed at fairly low temperatures in a tube with almost fully-developed flow. This made radiation negligible and the evaporation rates almost constant over the liquid film length. For these reasons the evaporation rate could be calculated by hand using the formulation of Section 2.4.1. For completeness the computer program was used to include the slight effects of radiation, interface motion, and boundary layer development.

The static pressure varied from 1.4 to 2.47 atm over the runs. An average saturation temperature of 240 F is stated by Kinney, corresponding to a saturation pressure of 1.7 atm. However, a liquid interface temperature of 200 F is given in Kinney's Figure 4. This difference might be attributed to mass transfer to the unsaturated gas. A pressure of 1.7 atm and an interface temperature of 200 F was assumed in all of the calculations, since no itemization was given for each run.

The free stream gas consisted of the products of gasoline/air combustion. For property values, pure air was assumed. For radiation calculations 10% CO_2 and 10% H_2O were assumed for all runs. In any event, radiation was insignificant at the low temperatures of the tests. Since the free stream turbulence was unknown, a value of 0% was used. The property values common to all runs were:

Gas:	Coolant:	
air	water	
M= 29.	M= 18.	μ= 3.03 10^{-4} kg/m-s
P= 1.7 atm	Tv= 366 K	ρ_l= 962 kg/m3
	Tc= 300 K	ρ_v= 1.01 kg/m3
	Cpl= 4210 J/kg-K	σ= 60.3 10^{-3} N/m
	λ= 2.27 10^8 J/kg	α= 0.

The property values of air are listed below (Reference 54) for each free stream gas temperature used in Kinney's tests.

Tg (F)	800	900	1200	1400	1600
Tg (K)	700	756	922	1033	1144
ρ_g (kg/m3)	0.857	0.794	0.651	0.582	0.525
μ_g (10^{-5} kg/m-s)	3.349	3.515	3.976	4.264	4.550
at T_{mean} (K) =	533	561	644	700	755
Cpg (J/kg-K)	1036	1042	1062	1075	1088
μ_g (10^{-5} kg/m-s)	2.80	2.90	3.17	3.35	3.51
Pr	0.698	0.698	0.701	0.702	0.703

Kinney stated only the free stream Reynold's numbers. Using the viscosity values above, the gas mass flux (G_{ch}) for each test was back-calculated from the stated Reynold's number. The liquid film length (L_c) at an average coolant flow $\Gamma = 0.08$ kg/s-m was determined for each test and the average evaporation rate calculated as: $\dot{m}_v = \Gamma/L_c$

Similarly, the experimental evaporation rates for both normal evaporation ($\dot{m}v_{exp_1}$) and after transition to the large waves ($\dot{m}v_{exp_2}$) were calculated from the slopes of the data plots in Kinney's Figure 6, giving:

TEST	Re_D (10^5)	G_{ch} (kg/s-m²)	L_C (cm)	$\dot{m}vcalc$ [	$\dot{m}vexp_1$ kg/s-m²	$\dot{m}vexp_2$]
2 in smooth:						
800F	4.4	290.1	86.6	0.0924	0.141	---
800F	5.6	369.2	71.3	0.112	0.200	---
1200F	3.5	273.9	50.8	0.157	0.236	0.450
1600F	2.5	223.9	38.5	0.208	---	0.611
4 in smooth:						
900F	6.0	207.6	106.7	0.0750	0.0794	0.326
900F	8.2	283.7	83.1	0.0963	0.109	0.226
900F	9.9	342.5	71.5	0.112	0.153	0.366
1400F	5.3	222.4	54.7	0.146	---	0.440
1600F	4.7	210.5	48.0	0.167	---	0.629
4 in rough:						
800F	6.8	224.1	119.9	0.0668	0.131	---
800F	11.0	362.6	81.5	0.0982	0.226	0.458
1400F	5.4	226.6	53.9	0.149	0.326	0.930
1400F	6.7	281.2	45.4	0.176	---	0.896

Comparison between the calculated and experimental (mv_{exp_1}) values is given in Figure 7. While the calculations do not compare favorably with all of the measurements in an absolute sense, they do correlate the data well. The calculated evaporation rates are a factor 35% lower than the data for the two "smooth" tubes. Assuming a free stream turbulence intensity of 8.75% would account for this discrepancy, as discussed in Section 2.1.1.

Several other factors could contribute to the discrepancy. Most significant is that the actual propellant flow rates were not stated, so that the gas mass flux (G_{ch}) had to be back-calculated without knowing the value of gas viscosity Kinney used in calculating the stated Reynold's numbers. Also, the specific heat of the actual combustion products is slightly higher than that for the pure air assumed. Finally, the "pebbling" of the liquid surface observed by Kinney would give an effect similar to pipe roughness, increasing the convective heat flux.

The model is not able to predict the evaporation rates when large waves are present, given by the mv_{exp_2} values. When the large waves are present, the rates of mass loss are increased by a factor of 2.56, on average.

4.1.2 E.L. Knuth air-water tests (Reference 18)

These tests were performed shortly after Kinney in a 2.9 inch diameter tube with fully-developed flow. The gas properties are again taken as those of pure air. 10% CO_2 and 10% H_2O in the products is assumed for the radiation calculations. The liquid interface temperature is taken as 339 K, based upon Knuth's Figure 11. This disagrees with the stated static pressure of 1 atm. The discrepancy is attributed to mass transfer to the unsaturated gas. The common properties used were:

Gas:	Coolant:	
air	water	
M= 29.	M= 18.	$\mu= 4.26 \ 10^{-4} \, kg/m\text{-}s$
P= 1 atm	Tv= 339 K	$\rho_l= 980 \ kg/m3$
	Tc= 300 K	$\rho_v= 0.1664 \ kg/m3$
	Cpl= 4188 J/kg-K	$\sigma= 65.1 \ 10^{-3} \, N/m$
	$\lambda= 2.34 \ 10^6 \, J/kg$	$\alpha= 0.$

The gas properties used in each calculation were (Reference 54):

TEST	20-30:	45-54:	89-99:
Tg (K)	613	901	1230
ρ_g (kg/m3)	0.576	0.392	0.287
at T_{mean} (K) =	476	620	785
Cpg (J/kg-K)	1025	1056	1095
μ_g (E-5kg/m-s)	2.59	3.10	3.60
Pr	0.699	0.700	0.703

With these property values, the liquid film lengths and evaporation rates for each test were determined at a coolant flow of 0.08 kg/s-m. Unlike Kinney, Knuth gave the mass flow of the freestream gas directly, eliminating one unknown.

TEST	G $(kg/s\text{-}m^2)$	Lc (cm)	$\dot{m}vcalc$ $(kg/s\text{-}m^2)$	$\dot{m}vexp$ $(kg/s\text{-}m^2)$
20-30	181.0	165.9	0.0482	0.0586
45-54	91.6	125.3	0.0638	0.0586
89-99	69.2	92.3	0.0867	0.0633

The calculated values agree fairly well with the measured values, however there is not enough data to generalize.

4.1.3 G. Morrell LOx/NH$_3$ rocket (Reference 52)

These test were performed in a 4 inch diameter rocket, with liquid oxygen and ammonia propellants. The liquid coolant was injected 2.8 inches downstream of the propellant injector. Water, ethanol and ammonia were tested as liquid coolants. The ammonia was at super-critical conditions and no sharp evaporation points were determined, hence it is omitted here. Since the free stream turbulence was not measured, a value of zero was used in the calculations.

The pressure varied from 16.9 to 17.7 atm in the water tests. For simplicity the following saturated coolant properties at 17.4 atm were used in all calculations:

coolant	T_v (K)	λ $\left[10^6 \frac{J}{kg}\right]$	C_{pl} $\left[\frac{J}{kg-K}\right]$	μ_v $\left[10^{-6}\frac{kg}{m-s}\right]$	μ_l	σ $\left[10^{-3}\frac{N}{m}\right]$	ρ_l $\left[\frac{kg}{m^3}\right]$	ρ_v	Γ_{cr} $\left[\frac{kg}{m-s}\right]$
water	480	1.91	4530	15.9	129	36.2	857	9.09	0.198
ethanol	448	0.574	5126	13.1	121	7.91	637	27.6	0.143

The properties for water are from Reference 54. Most of the ethanol properties are from Reid (Reference 55): T_v is from Appendix A, λ from Equation 7-9.4, ρ_l from Equation 3-11.9, μ_v from Table 9-2, and μ_l from Table 9-8. The remaining ethanol properties (C_{pl}, σ, and ρ_v) are from various tables in Perry's Handbook (Reference 56).

The free stream gas differed in composition for each run, with the O/F mass ratio given by Morrell. The water coolant tests were all lean, with a reaction:

$$x_1 NH_3 + x_2 O_2 \rightarrow 1.5x_1 H_2O + \tfrac{1}{2}x_1 N_2 + (x_2 - 0.75x_1)O_2$$

The water vapor fraction, x_{H_2O}, was related to the O/F mass ratio by:

$$x_{H_2O} = 48/[40+17(O/F)]$$

The molecular weight of the products was calculated as:

$$Mg = \frac{544[1+(O/F)]}{40+17(O/F)}$$

The following properties were used for each product species in the gas, at a mean temperature of 1720 K:

	C_p (J/kg-K)	μ_g $(10^{-5}$ kg/m-s)	Pr
H_2O:	2684	5.85	0.9
N_2 :	1266	5.61	0.708
O_2 :	1167	6.78	0.75

The specific heats were calculated from Table 3-2 of Holman (Reference 57) for low pressure. From Holman's Figure 7.8, the corrections for chamber pressure are negligible. The viscosities were calculated from the Chapman-Enskog correlation, using the values in Appendix B of Reid (Reference 55). The Prandtl numbers were extrapolated from the charts in Appendix A of Kays (Reference 5).

The viscosity of the products was calculated at an O/F mixture of 1.61, using the mixture weighting of Wilke (Reference 55, Eq. 9.5-13), giving: $\mu_g = 5.86 \ 10^{-5}$ kg/m-s. The specific heats were weighted by the mass fractions of the product species and the Prandtl numbers by the mole fractions for each run. With these property values the liquid film lengths were calculated for each test:

Test	O/F	T_g (K)	P (atm)	G $\left[\dfrac{kg}{s\text{-}m^2}\right]$	C_{pg} $\left[\dfrac{J}{kg\text{-}K}\right]$	Pr	Γ $\left[\dfrac{kg}{s\text{-}m}\right]$	$L\vert_{meas}$ (cm)	$L\vert_{calc}$ (cm)
water:									
1	1.61	2950	17.4	226	2120	0.847	0.269	21.2	24.9
2	1.56	2960	17.8	234	2141	0.848	0.258	19.4	23.0
3	1.64	2945	17.0	225	2110	0.846	0.213	14.2	19.6
4	1.42	2978	17.4	233	2196	0.852	0.219	14.6	18.9
5	1.50	2963	17.0	207	2164	0.850	0.209	16.2	19.8
6	1.66	2940	17.1	229	2104	0.846	0.130	7.01	11.45
7	1.72	2935	17.5	220	2082	0.844	0.128	9.86	11.65
8	1.41	2978	17.1	209	2199	0.852	0.262	18.8	24.6
9	1.51	2963	16.9	214	2159	0.849	0.262	20.7	24.8
10	1.75	2930	17.7	225	2072	0.844	0.290	20.4	27.7
11	1.67	2942	17.7	224	2100	0.845	0.296	21.7	28.0
ethanol:									
12	1.18	"	17.8	223	"	"	0.809	14.2	50.0
13	1.10	"	17.4	222	"	"	0.869	16.2	54.4
14	1.17	"	17.8	225	"	"	0.834	17.4	51.4
15	1.12	"	17.4	211	"	"	0.859	19.4	55.2
17	1.25	"	18.0	209	"	"	0.872	17.7	56.1
18	1.17	"	17.7	228	"	"	0.869	18.0	53.4
19	1.13	"	17.6	224	"	"	0.716	16.2	43.8
20	1.25	"	18.0	224	"	"	0.713	16.2	43.5
22	1.41	2978	18.1	236	2199	0.852	0.570	14.6	33.1
23	1.37	"	17.9	225	"	"	0.598	15.8	35.9
25	1.48	"	18.1	230	"	"	0.535	11.0	31.4
26	1.31	"	18.2	237	"	"	0.525	10.4	30.2
28	1.54	"	18.0	238	"	"	0.341	10.3	19.0
29	1.53	"	17.8	225	"	"	0.369	9.55	21.4
30	1.59	"	18.2	231	"	"	0.318	10.2	17.9

A comparison of the calculations with the experimental data for water coolant is given in Figure 8. The calculated liquid film lengths are an average of 25% longer than measured. Since convection accounted for 62% of the total evaporation rate, multiplying the convective heat flux by a factor of 1.4 would bring the calculations into best agreement with the measurements. This corresponds to a free stream turbulence of 9%, which is a reasonable assumption.

In all of the ethanol tests the liquid coolant flow rate (Γ) greatly exceeded Knuth's critical value for the formation of large waves (Γ_{cr}), given in the coolant table above. Such large waves would explain why the measured liquid film lengths were an average of 2.75 times shorter than calculated, which compares favorably with Kinney's results for the mass loss rate with large waves present. For simplicity, the gas properties at an O/F of 1.41 were used in all of the ethanol calculations.

Katto's correlation for radiant burnout is tested in the program and predicted liquid film lengths 10% shorter than listed above with water coolant. However, with ethanol coolant the burnout condition predicted liquid film lengths of less than 1 cm, which is unreasonable. Therefore the burnout prediction was not deemed trustworthy.

4.1.4 Warner and Emmons H_2/air rocket (Reference 34)

These tests were made in a 79.8 mm diameter rocket chamber burning air and H_2. The liquid film cooling test section was 276 mm downstream of the injector. The data given in their Figure 5 was analyzed. The gas was assumed due to the stoichiometric reaction of air and H_2, giving 0.653 N_2 and 0.347 H_2O molar fractions, and a molecular weight of 24.5. A temperature of 2222 K and a pressure of 34 atm were reported.

Since the mass flow of gas (G_{ch}) was not given, it was back-calculated from the stated Reynold's number of 68,000. At the free stream temperature the species viscosities were $6.626 \ 10^{-5}$ kg/m-s for N_2 and $7.186 \ 10^{-5}$ kg/m-s for H_2O. Using Wilke's method, the free stream gas viscosity was $6.806 \ 10^{-5}$ kg/m-s. Using this value: $G_{ch} = 58.03$ kg/s-m^2.

The gas properties, evaluated at a mean temperature of 1300 K, are listed below:

	C_p (J/kg-K)	Pr	μ (10^{-5} kg/m-s)
N_2	1226	0.705	4.680
H_2O	2494	0.90	4.584
mixture	1549	0.773	4.670

The property values were determined in the same manner as for Morrell's data.

Three different coolants were tested. The properties of each at the chamber pressure are given below:

coolant	Tv (K)	λ $\left[10^{8}\dfrac{J}{kg}\right]$	C_{pl} $\left[\dfrac{J}{kg-K}\right]$	μ_v $\left[10^{-6}\dfrac{kg}{m-s}\right]$	μ_l	σ $\left[10^{-3}\dfrac{N}{m}\right]$	ρ_l $\left[\dfrac{kg}{m^3}\right]$	ρ_v	Γ_{cr} $\left[\dfrac{kg}{s-m}\right]$
water	514	1.76	4779	17.1	111.0	28.4	813	17.0	0.266
ethanol	480	0.440	5126	14.0	83.0	4.18	564	50.3	0.239
ammonia	345	0.937	4103	11.9	79.4	10.25	523	25.2	0.180

The coolant properties were determined as in Morrell's tests, with the exceptions that λ, C_{pl}, ρ_l, and ρ_v for ammonia were scaled from the values at 325 K in Table 3-209 of Perry (Reference 56).

With these property values, the liquid film length and average evaporation rates for each test were calculated at a coolant flow (Γ) of 0.08 kg/s-m, giving:

Coolant	L_c (cm)	$\dot{m}_{vcalc}$ (kg/s-m^2)	$\dot{m}_{vexp}$ (kg/s-m^2)
water	29.05	0.275	0.439
NH3	14.25	0.561	1.159
ethanol	16.85	0.475	0.886

Both the ammonia and ethanol data are somewhat questionable since they extrapolate to a positive coolant flow at zero film cooled length, indicating an initial mass loss at injection. The ammonia data also showed significant scatter. The flow rates in the ammonia tests were centered about Knuth's critical value, which may explain the scatter.

The calculated evaporation rate for water coolant is 37% lower than measured. Radiation accounted for 62.8% of the calculated evaporation rate, making the calculations very sensitive to the assumed gas temperature. Given the uncertainties in the test conditions, it is futile to speculate at length as to the discrepancy.

4.1.5 R.C. Kesselring, et al OF_2/B_2H_6 rocket test (Reference 53)

These tests were performed in a rocket engine using diborane fuel, which is uncommon and very expensive. The combustion chamber was a thin nickle shell of 9.45 cm diameter, used for short duration tests. The free stream gas conditions were fairly constant for all runs, so that the average properties below were used in analyzing all runs:

$T_g = 3900$ K, $P = 6.8$ atm, $G_{ch} = 150.7$ kg/s·m^2 .

The NASA/Lewis Chemical Equilibrium code gave the following free stream mole fractions and properties:

0.537 HF, 0.225 BOF, 0.063 H_2O, 0.036 H_2, 0.031 OH, $M_g = 25.6$

and at $T_{mean} = 2200$ K:

$C_{pg} = 3665$ J/kg-K, $\mu_g = 8.37\ 10^{-5}$ kg/m-s, $Pr = 0.80$

The properties of saturated B_2H_6 coolant at 6.94 atm from Kit and Evered (Reference 58) are:

$T_v = 243.8$ K, $M_c = 27.69$, $\lambda = 3.72\ 10^5$ J/kg, $C_{pl} = 3235$ J/kg-K
$\mu_l = 3.6\ 10^{-5}$ kg/m·s, $\rho_l = 341$ kg/m^3, $\rho_v = 29.4$ kg/m^3, $\sigma = 7.16\ 10^{-3}$ N/m

Kit and Evered give $\lambda = 5.173\ 10^5$ J/kg at $T_b = 180.04$ K at 1 atm, which compares well with Perry's handbook (Reference 56). Scaling λ as suggested in Reid (Reference 55) to 243.8 K, using $T_{crit} = 289.7$ K, gives the value above. The vapor viscosity was not found. However, due to the very low liquid viscosity, the critical flow rate for forming large waves, Γ_{cr}, is estimated to exceed 100 kg/m·s, making such waves unlikely.

Thermocouples were located on the outside of the thin chamber. A steady temperature rise during a run was indicative of the absence of liquid film on the wall at that axial position. Where the liquid film did exist the wall temperature actually decreased during a firing, due to the low saturation temperature of diborane. Unfortunately, the thermocouples were spaced 2 inches apart, making it difficult to determine the liquid film lengths accurately. The best approximations are given below:

TEST	Γ (kg/m-s)	Lc (in)
1	0.583	3< Lc <5
3	0.445	1< Lc <3
4	0.451	1< Lc <3
6	0.191	1< Lc <3
9	0.306	1< Lc <3
10	0.532	≈ 3
11	0.435	1< Lc <3

Surprisingly, the authors assume that the liquid is immediately evaporated, based upon calculations of the normally expected heat flux without transpiration. They interpret the thermocouple data as meaning that this vapor refrains from mixing with the hot gases until some arbitrary distance downstream.

No information on the emittance of the combustion products was available, so the emittance was treated as an adjustable parameter. Assuming 8% free stream turbulence, the best comparison between the data and calculations was obtained with an assumed emittance of 17%, as shown in Figure 9. Radiation accounted for 90% of the heat flux in this case. The calculated liquid film length is somewhat insensitive to the assumed emittance. For example, halving the emittance to 8.5% increases the calculated liquid film length by 58%, whereas an 82% increase might be expected. The reason is that the vapor liberated by radiation greatly decreases the convective heat flux through transpiration. If the radiative flux decreases, convection increases, keeping the evaporation rate somewhat constant.

Given the numerous species in the products, one might expect a larger emittance, however the optical density of 64 atm-cm was fairly low. To critically judge the analysis for this test requires an independent determination of the gas emittance.

4.2 GASEOUS FILM COOLING

4.2.1 Ewen and Rousar (References 49-51)

The goal in all three test programs was to study gaseous film cooling in a converging-diverging nozzle, for application to rocket engines. The authors analyzed their data in terms of an empirical model. Although their model is similar to the differential entrainment formulation of Section 3.4.1, it is not based upon standard correlations. For this reason only their raw data was used.

In the first two reports (1972 and 1973) testing was done on a flow bench in a laboratory, using heated nitrogen for the free stream flow and either hydrogen or nitrogen coolant. The free stream turbulence was measured to be 4.1% for all tests. The free stream flow was fully-developed upon contacting the coolant injector, leading to a difficulty in specifying the injection position from the "leading edge", a problem discussed later. Only those tests with a coolant injection velocity less than the free stream velocity were analyzed (to avoid jet effects), although all of the data was qualitatively similar. The test conditions are given below:

Test	chamber	G_{ch} $(kg/s \cdot m^2)$	T_g (K)	coolant	$\dot{M}_c$ $(kg/s \cdot m)$	T_c (K)	Δet $(\%)$
1972:							
3	30°-1R	630	763	H_2	0.189	294	38
5A	" "	629	764	H_2	0.185	285	28
8	" "	636	756	H_2	0.122	111	6
11A	conical	631	761	H_2	0.185	292	0
1973:							
101L	30°-1R	581	820	N_2	0.355	341	0
101H	" "	577	822	N_2	0.528	320	0
102	30°-2R	528	880	H_2	0.170	270	16
103A	15°-2R	591	816	H_2	0.173	275	18
104AL	" "	599	815	N_2	0.360	345	0
104AH	" "	596	817	N_2	0.677	327	0
105A	con. mod	597	817	H_2	0.157	270	0

For test 104AL, the free stream temperature was stated as 915° K in Rousar and Ewen's report, apparently as a misprint. Also, for tests 102, 103A, and 105A, the stated coolant injection temperatures, T_c, were adjusted to be consistent with the axial thermocouple readings.

In the last report (1977), measurements were made in an O_2 (g)/H₂ rocket engine using hydrogen, nitrogen, and helium coolants. All tests used the same chamber (P/N 1182134). The coolant injector was 178 mm downstream of the

propellant injector. The test conditions are given below:

Test	O/F	G_{ch} (kg/s·m²)	T_g (K)	coolant	$\dot{M}_c$ (kg/s·m)	T_C (K)	Δe_t (%)
102	3.89	242.6	2670	H2	0.587	290	0.
103	3.81	228.5	2640	H2	0.504	290	0.
105	5.75	241.3	2990	H2	0.478	290	0.
110	7.71	263.1	3080	H2	0.414	290	0.
111	7.99	260.6	3080	H2	0.362	290	0.
114	6.27	237.5	3030	H2	0.345	290	0.
115	5.93	234.9	3005	H2	0.408	290	0.
116	7.60	246.4	3075	H2	0.309	290	0.
117	4.00	219.5	2720	H2	0.391	290	0.
119	7.76	283.7	3080	He	0.515	310	0.
120	7.46	270.8	3075	He	0.469	310	0.
122	7.75	299.1	3080	He	0.595	310	0.

The coolant flow rates (W_C) were not given directly and were back-calculated from the stated total mass flow (W_T), the coolant to fuel mass flow ratio (W_C/W_F), and the O/F ratios as:

$$W_C = (W_C/W_F) \; W_T/(1+O/F)$$

The $\dot{M}_C$ values tabulated above are the coolant mass flows (W_C) per circumference.

In all of the tests the products contained excess hydrogen. From the reaction stoichiometry, the mass fraction of H_2O in the products is given by:

$$m_{H_2O} = 9/8 \; (O/F)/[1+(O/F)]$$

the remainder being H_2. The flame temperatures, T_g, listed are from a plot of somewhat conflicting values from a number of literature sources, mostly at 1 atm pressure.

The specific heats of the various gas species were calculated as (Reference 57):

$$C_p|_{N_2} = 1415 - 2.88 \; 10^5 K/T + 53.48 \; 10^6 K^2/T^2 \quad J/kg \cdot K$$
$$C_p|_{H_2} = 12,047 + 2.176 K^{-1} \; T + 31,180 K^{\frac{1}{2}}/T^{\frac{1}{2}} \quad J/kg \cdot K$$
$$C_p|_{H_2O} = 4615 - 1.03 \; 10^5 K^{\frac{1}{2}}/T^{\frac{1}{2}} + 9.68 \; 10^5 K/T \quad J/kg \cdot K$$
$$C_p|_{He} = 5238 \; J/kg \cdot K$$

These specific heats were weighted by the species mass fractions to determine the product specific heats.

The viscosity of each species was calculated from the Chapman-Enskog constants. The mixture weighting method of Wilke was used to determine the product viscosity (Reference 55):

$$\mu|_{N_2} = 1.23 \; 10^{-6} \; \sqrt{T} \quad kg/m \cdot s$$
$$\mu|_{H_2} = 6.71 \; 10^{-7} \; \sqrt{T} \quad kg/m \cdot s$$
$$\mu|_{H_2O} = 8.22 \; 10^{-7} \; \sqrt{T} \quad kg/m \cdot s$$

The parameters describing the chamber contours, discussed in Section 3.6, are tabulated below:

chamber	D_{ch} (mm)	l_1 (mm)	r_1 (mm)	θ_c (deg)	D_t (mm)	r_2 (mm)	θ_d (deg)
30°-1R	31.	88.9	15.5	30.	15.5	7.8	15.
30°-2R	31.	88.9	31.	30.	15.5	15.5	15.
15°-2R	31.	88.9	31.	15.	15.5	15.5	15.
conical	31.	7.9	12.7	4.4	15.5	7.8	15.
(modified)	31.	0.	12.7	4.4	15.5	7.8	15.
1182134	99.6	106.7	51.8	30.	52.1	28.7	15.

The results of each calculation are compared with the data in Figure 10. The simplest geometry was test 11A, with a gradually converging conical chamber. For comparison, the calculations are shown both with the differential entrainment formulation (Section 3.4.1) and with the simpler integral correlation (Section 3.0) (based upon the starting conditions). The injection point was assumed at $x_{in} = 0$ for both. The differential formulation gives the best comparison up to the throat. Downstream of the throat the wall temperature decreases much faster than predicted by the model, a difficulty with all of the calculations which is discussed later.

The comparison is not as good for the cylindrical chamber data, such as for test 3. The wall temperature increases very rapidly downstream of the converging turn (at 88.9 mm). The calculated value might be expected to rise due to the increase in the free stream mass flow as the chamber area decreases. However, as shown by the solid curve, this is not the case. The reason is that the contraction also increases the boundary layer mass flow per circumference, as discussed in Section 3.4.2, and the two effects tend to cancel. Disabling this circumferential correction term yields a better comparison, as shown by the dashed curve. However, such fortuitous comparison is not a suitable reason for discounting a physical effect, so the circumferential term is left in the model.

As in most modeling efforts the comparison can be improved by judicious selection of input parameters, as shown in the second figure. To force comparison in the straight chamber section, a downstream injection point (x_{in}) of 20 mm was used. While arbitrary, this could be defended by arguing that in fully-developed flow the injection point is considered an infinite distance from the "leading edge". However, with the exception of tests 3 and 5A, $x_{in} = 0$ was always the optimum choice. This is supported by heat transfer data taken by Ewen and Rousar which show the initially high convective heat transfer rates of a leading edge at the injection point. Apparently the coolant injection disrupts the flow such that a new boundary layer grows from the injection point.

To force comparison downstream of the converging turn it was necessary to assume an increase in the free stream turbulence due to the turn, Δe_t, of 38% for test 3. Similar correction factors are necessary with all turbulence models (Reference 59). The values required for each test are tabulated above.

Such a correction is defensible only if it is not arbitrary. This extra "turning turbulence" can be correlated by a "centrifugal parameter":

$$F_c = (\rho_g - \rho_c)\frac{V^2}{r_1} = \frac{G^2}{r_1 \rho_g}\left[1 - \frac{\rho_c}{\rho_g}\right]$$

where r_1 is the radius of the converging turn, ρ_c and ρ_g are the coolant and gas densities at the turn. Note that F_c has dimensions. For all of the 1977 tests in the rocket engine, the correction was negligible. Given the low densities in most rocket chambers, this is generally true.

As shown in Figure 11, the correlation between Δe_t and F_c can be fit by a function:

$$\Delta e_t = 5.26 \left\{[1 + (0.029\ F_c)^6]^{1/6} - 1\right\} \quad \text{for } \rho_g > \rho_c$$
$$= 0. \quad \text{for } \rho_g < \rho_c$$
$$\text{where:} \quad F_c <> kN/m^3$$

The aberrant point is due to test 8 of 1972, for which it was impossible to obtain any satisfactory comparisons.

It was not possible to obtain a reasonable comparison with the data of tests 119-122 which used helium coolant. The rate of temperature rise with non-reactive helium coolant was overpredicted by a factor of 1.7, raising the question that combustion effects are important and that the favorable comparisons with hydrogen coolant in the rocket were merely fortuitous.

For instance, the free stream temperature close to the wall might have been considerably less than that used in the calculations above. Since many injectors provide a fuel rich zone near the wall, this is plausible. Such an assumption would make the He coolant calculations compare more favorably with the data. Normally this assumption would also lead to a significant under-prediction of the wall temperatures with H_2 coolant. However, considering combustion of the H_2 coolant in the boundary layer could restore the wall temperatures to the measured values. Data with other coolants is needed to ascertain whether combustion effects could explain the discrepancy.

In all of the calculations it was not possible to account for the rapid decrease of wall temperature downstream of the throat. Since the wall temperature decreased even faster than the free stream gas static temperature, increased mixing with the free stream gases could not account for this rapid decrease. Instead, it might be attributed to the static temperature change of the boundary layer gases as they accelerate. Since the present formulation lumps together all of the boundary layer gases, it would be difficult to incorporate such an effect into the model. A turbulent boundary layer model, which considers the velocity profile across the boundary layer, would be better suited to this task.

All of the calculated results assumed a recovery factor of zero, meaning that the entrained free stream gas is at the static temperature. However, upstream of the nozzle throat there is little difference between the static and stagnation temperatures, so that the choice of recovery factor is not significant. Downstream of the throat the present model is unable to accurately predict the wall temperature, regardless of the choice of recovery factor.

AEDC-TR-91-1

4.2.2 G.R. Kinney, et al (Reference 17)

The data in this report was reviewed in Section 4.1.1 pertaining to calculation of liquid film lengths, which was the focus of their study. The authors do, however, give one plot of temperatures downstream of the dryout point in their Figure 4. This data is useful in determining how to apply the gaseous film cooling analysis to the special case of liquid film cooling. The property values are from Section 4.1.1 .

The start of the liquid film was 40 inches from the tube entrance, and the liquid film was 20 inches long. As argued in the previous analysis of Ewen and Rousar's data, the gaseous coolant injection tends to disturb the boundary layer such that the injection point acts effectively as a "leading edge". The simplest assumption is that all of the vapor is injected at the termination of the liquid film ($x_{in}=0$). The calculated wall temperatures compare favorably with the data, as shown in Figure 12. This is compared with an alternate assumption that the effective leading edge is in the center of the liquid film ($x_{in} = 254$ mm), which gives very poor comparison with the data. Therefore, as was found with Ewen and Rousar's data, taking $x_{in} = 0$ generally gives the best comparisons with existing data for all cases.

5.0 CONCLUSIONS

A simple one-dimensional model gives satisfactory comparison with existing data for liquid film lengths in rocket engines. Convective and radiant heat transfer must both be considered. At high coolant flow rates large waves on the film can decrease the coolant efficiency. Knuth's correlation is useful in predicting this transition. Radiant burnout of the liquid film is possible, however the use of existing burnout correlations is questionable.

Downstream of the liquid film a standard gaseous film cooling correlation, modified to a differential form, satisfactorily predicts the wall temperatures upstream of the throat as the vapor mixes with the free stream gas. A correction factor, correlated in terms of a "centrifugal parameter", is needed to account for increased mixing due to the converging turn. However, in most rocket engines it is not significant. Downstream of the throat the wall temperature drops very rapidly due to acceleration of the boundary layer gases, which is not predicted by the present model.

REFERENCES

1. Cebeci,T. and Bradshaw,P. Physical and Computational aspects of Convective Heat Transfer. Springer-Verlag, 1984.
2. Schlichting, H. Boundary Layer Theory. McGraw-Hill, 1981.
3. Landis, R.B. "Numerical Solution of Variable Property Turbulent Boundary Layers with Foreign Gas Injection". PhD Thesis, UCLA, 1971.
4. Reynolds, W.C., et. al. NASA Memo 12-1-58W, 1958.
5. Kays, W.M. Convective Heat and Mass Transfer. McGraw-Hill, 1966.
6. Humble, L.V., et. al. NACA Report 1020, 1951.
7. Bartz, D.R. "A Simple Equation for Rapid Estimation of Rocket Nozzle Convective Heat Transfer Coefficients", Jet Propulsion - ARS Journal, Jan. 1957, p. 49 .
8. Churchill, S.W. and Usagi, R. "A General Expression for the Correlation of Rates of Transfer and other Phenomena", AIChE Journal. Vol. 18, No. 6, (Nov. 1972), pp 1121-1128.
9. Barbin, A.R. and Jones, J.B. "Turbulent Flow in the Inlet Region of a Smooth Pipe", Trans. ASME - Journal of Basic Engineering. March 1963, p. 29.
10. Pletcher, R.H. "Progress in Turbulent Forced Convection", Trans. ASME - Journal of Heat Transfer. Vol. 110, Nov. 1988, p. 1129.
11. Hersch, M. ARS Journal. Vol. 31, (1961), p. 39 .
12. Talmor, E. A.I.Ch.E. Journal, Vol. 12, (1966), p. 1092 .
13. Hartnett, J.P. et. al. in Heat and Mass Transfer in Boundary Layers. Vol.1 N. Afgan, editor, Pergamon, 1972.
14. Bird,R.B., Stewart, W.E., and Lightfoot, E.N. Transport Phenomena. Wiley (1960)
15. Brunner, M. J. ASME Paper no. 64-WA/HT-50.
16. Rubesin, M.W. et al. Handbook of Heat Transfer. W.M. Rosenhow, editor. McGraw-Hill, Ch. 8, p. 171.
17. Kinney, G.R. et al. "Internal Liquid Film Cooling Experiments with ..." NACA Report 1087, 1952.
18. Knuth, E.L. "The Mechanics of Film Cooling". JPL Memo 20-85, September 1953.
19. Gater, R.A. et al. Jet Propulsion Center TM-69-1, Purdue Univ., contract Nonr 1100(21), 1969.
20. Hanratty, T.J. and Hersham, A. "Initiation of Roll Waves", AIChE Journal, vol. 7, no.3, Sept. 1961, p. 488.
21. Woodmansee, D.E. and Hanratty, T.J. "Base Film over which Roll Waves Propogate", AIChE Journal, vol. 15, no. 5, Sept. 1969, p. 712.
22. Tatterson, D.F., et. al. "Drop Sizes in Annular Gas-Liquid Flows", AIChE Journal, vol. 23, no. 1, Jan. 1977, p. 68.

23. Research Summary No. 36-4, Volume II. Jet Propulsion Laboratory, Pasadena, California, September 1, 1960. pp 82-84.

24. Sutton, G.P. et al. "Advanced Cooling Techniques for Rocket Engines", Astronautics and Aeronautics, January 1966, pp 60-71.

25. Siegel, R. and Howell, J.R. Thermal Radiation Heat Transfer, second edition, Hemisphere, (1981), Section 17.5 - 17.6 .

26. Ziebland, H. and Parkinson, R.C. "Heat Transfer in Rocket Engines", AGARD-AG-148-71, Sept 1971, Ch.6 .

27. Burrows, M.C. NASA TND - 2541, 1964.

28. Monde, M. and Katto, Y. "Burnout in a High Heat Flux Boiling System with an Impinging Jet", Int. Journal of Heat and Mass Transfer, Vol.21, 1978, p.295.

29. Katto, Y. and Ishii, K. "Burnout in a High Heat Flux Boiling System with a forced supply of liquid through a Plane Jet", 7th Int. Heat Transfer Conf., Vol.4, Toronto, 1978, p.435.

30. Mudawwar, I.A., Incropera, T.A. and F.P. "Critical Heat Flux in Falling Liquid Films". Particulate Phenomena and Multiphase Transport, T.N. Veziroglu, ed., Volume 2, Hemisphere, 1988.

31. CPIA Liquid Propellants Manual, Chemical Propulsion Information Agency, Laurel, Md.

32. Zucrow, M.J. and Graham, A.R. "Some Considerations of Film Cooling for Rocket Motors", Jet Propulsion - ARS Journal, June 1957, p. 650.

33. Zucrow, M.J. and Sellers, J.P. "Experimental Investigation of Rocket Motor Film Cooling", ARS Journal, May 1961, p. 668.

34. Warner, C.F. and Emmons, D.L. "Effects of Selected Gas Stream Parameters and Coolant Properties on Liquid Film Cooling", Trans. ASME Journal of Heat Transfer, May 1964, p. 271.

35. Gater, R.A. et al. Jet Propulsion Center TM-65-6, Purdue Univ., Contract Nonr 1100(21), October 1965.

36. Shembharkar, T. R. and Pai, B.R. "Prediction of Film Cooling with a Liquid Coolant", Int. Journal of Heat and Mass Transfer, Vol. 29, No. 6, 1986, p. 899.

37. Economos, C. "The Compressible Turbulent Boundary Layer with Mass Transfer". Phd thesis, Polytechhnic Inst. of Brooklyn, 1968.

38. Kutateladze,S.S. et al. High Temperature (Soviet),Vol.1, Sept-Oct 1963.

39. Stollery, J.L. and El-Ehwany, A.A.M. "A note on the use of a Boundary Layer Model for correlating Film Cooling Data", Int. Journal of Heat and Mass Transfer, Vol.8, 1965, p.55 .

40. Hatch, J.E. and Papell, S.S, NASA TND-130, 1959.

41. Librizzi, J. and Cresci, R.J. "Transpiration Cooling of a Turbulent Boundary Layer in an Axisymmetric Nozzle", AIAA Journal, Vol.2, No.4, April 1964.

42. Goldstein, R.J. et al. "Film Cooling Effectiveness with Injection through a Porous Section", Trans. ASME Journal of Heat Transfer, August 1965, p.353 .

43. Goldstein, R.J. et al. "Film Cooling with Helium Injection into an Incompressible Air Flow", Int. J. of Heat and Mass Transfer, Vol. 9, 1966, p.1341.

44. Marek, C.J. Tacina, R.R. "Effect of Free-stream Turbulence on Film Cooling", NASA TN D-7958, June 1975.

45. Carlson, L.W. and Talmor, E. "Gaseous Film Cooling at Various Degrees of Hot Gas Acceleration and Turbulence Levels", Int. Journal of Heat and Mass Transfer, Vol.11, 1968, p. 1695.

46. Burns, W.K. and J.L. Stollery, "The Influence of Foreign Gas Injection and Slot Geometry on Film Cooling Effectiveness", Int. J. of Heat and Mass Transfer, Vol. 12 1969, p. 935.

47. Hartnett, J.P. et al in Handbook of Heat Transfer. W.M. Rosenhow, editor, McGraw-Hill, Ch. 17, Sec. B.2, 1973.

48. Eckert, E.R.G. and Drake, R.M. Analysis of Heat and Mass Transfer. McGraw-Hill, 1972.

49. Ewen, R.L. "Hydrogen Film/Conductive Cooling", NASA CR-120926, November 1972 (Aerojet).

50. Rousar, D.C. and Ewen, R.L. "Hydrogen Film Cooling Investigation", NASA CR-121235, August 1973 (Aerojet).

51. Rousar, D.C. and Ewen, R.L. "Combustion Effects on Film Cooling", NASA CR-135052, February 1977 (Aerojet).

52. Morrell,G. "Investigation of Internal Film Cooling of 1000 lb Thrust Liquid Ammonia, Liquid Oxygen Rocket Engine Combustion Chamber", NACA RM E51E04, July 1951.

53. Kesselring,R.C. et al. "Boundary Cooled Rocket Engines for Space Storable Propellants". NAS7-767, NASA-CR-129260, June 1972, (Rocketdyne).

54. Brodkey, R.S. and Hershey, H.C., Transport Phenomenon - a unified approach. Tables A.1 and A.2 McGraw-Hill, 1988.

55. Reid, R.C. et. al. The Properties of Gases and Liquids. 4th ed. McGraw-Hill (1987)

56. Perry, ed. Chemical Engineer's Handbook. McGraw-Hill.

57. Holman, J.P. Thermodynamics. 2nd ed., McGraw-Hill (1974)

58. Kit, B. and Evered, D.S. Rocket Propellant Handbook. MacMillan (1960)

59. Gibson, M.M. and Younis, B.A. "Modeling the Curved Turbulent Wall Jet", AIAA Journal, 20, no. 12, December 1982.

...
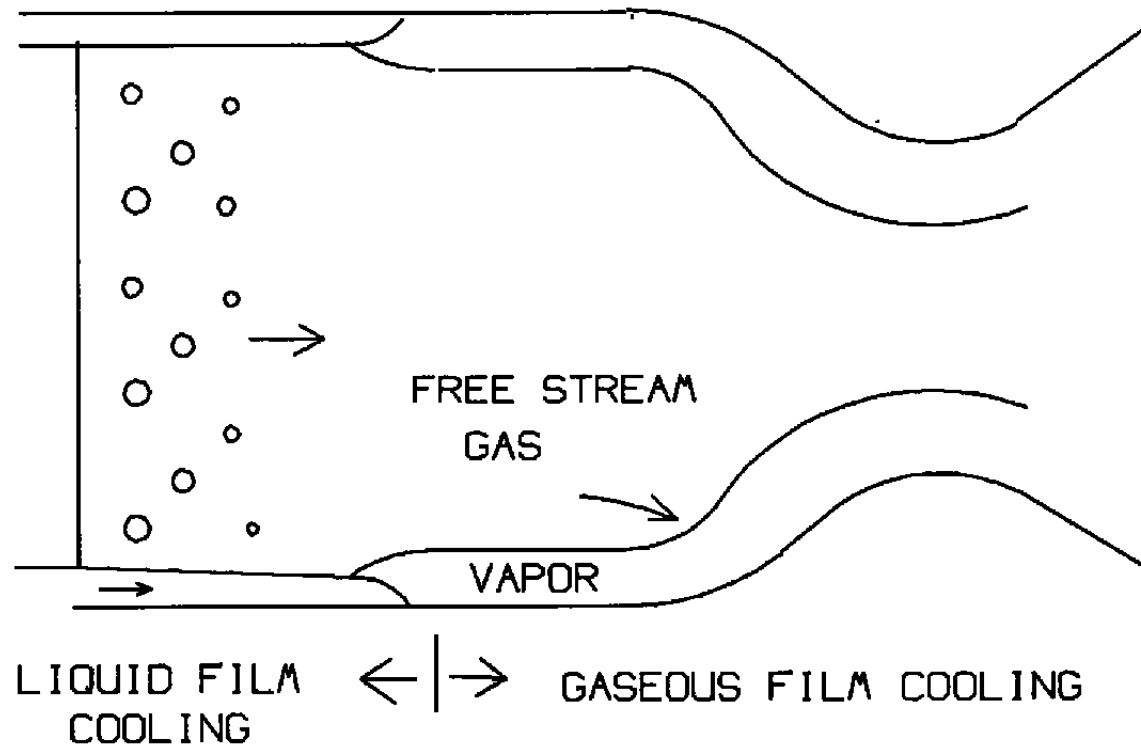
Figure 1. Mechanics of liquid film cooling.

LIQUID FILM COOLING $\longleftarrow | \longrightarrow$ GASEOUS FILM COOLING

FREE STREAM GAS

VAPOR
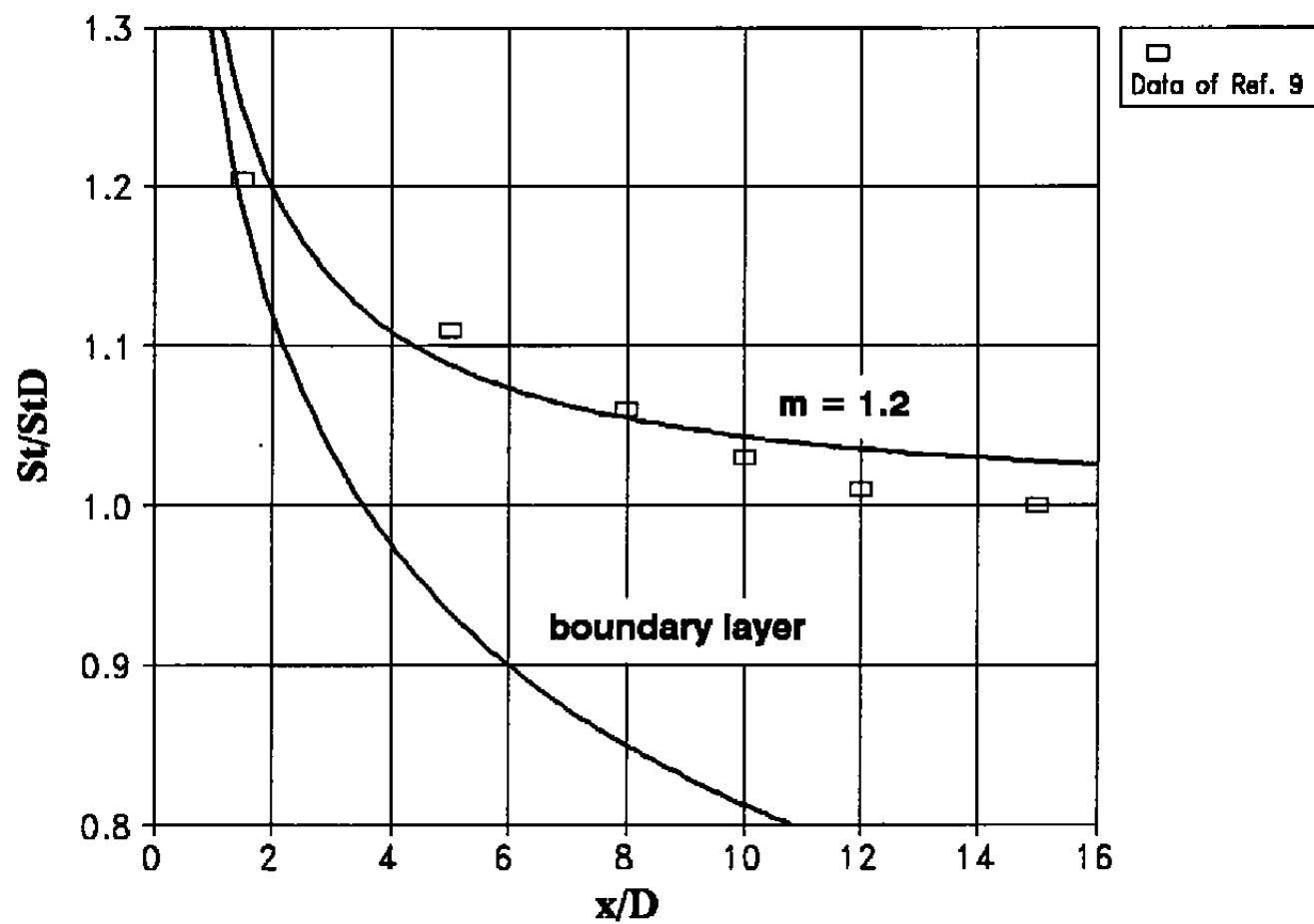
Figure 2. Transition to fully-developed flow.
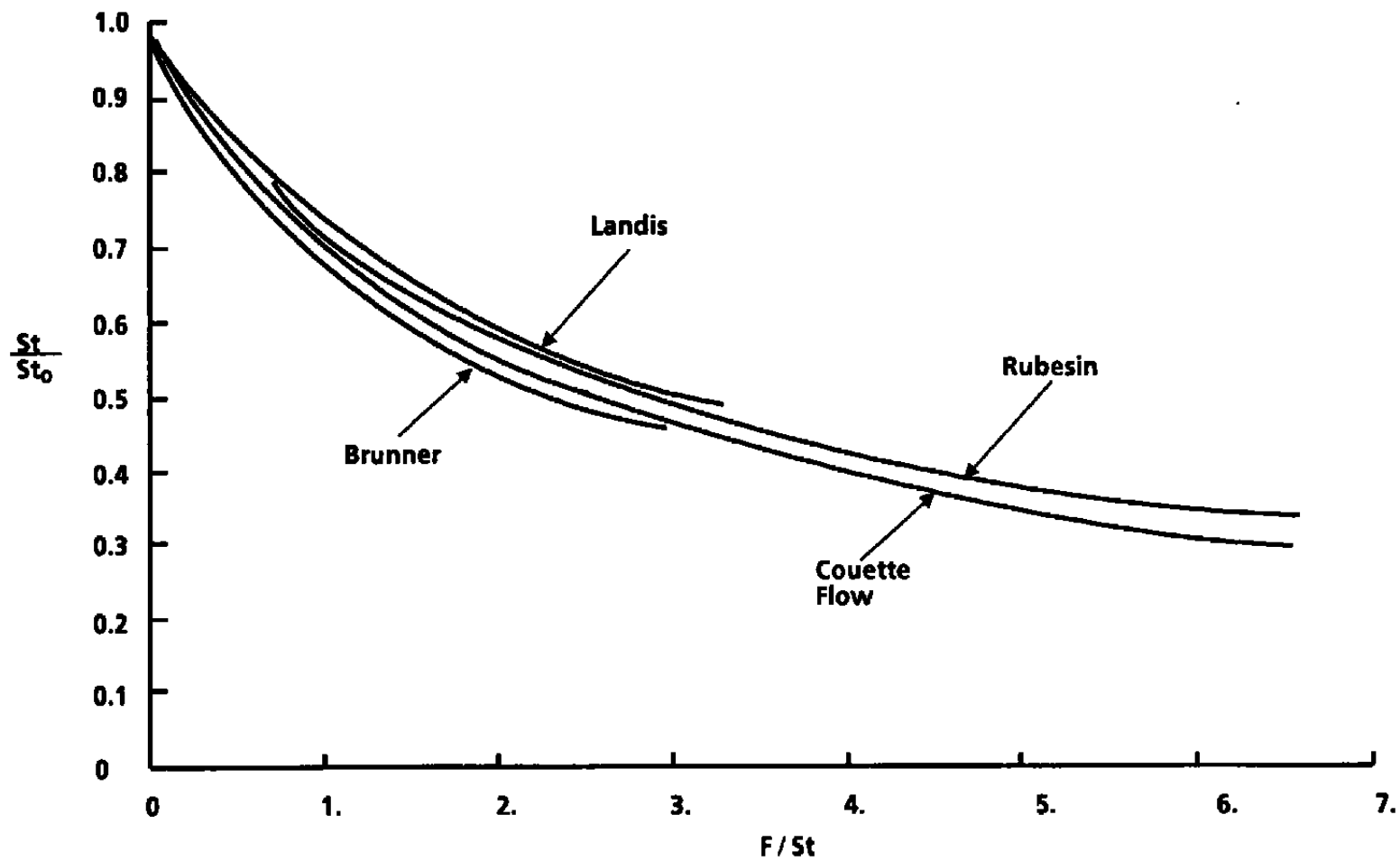
Figure 3. Comparison of transpiration relations.
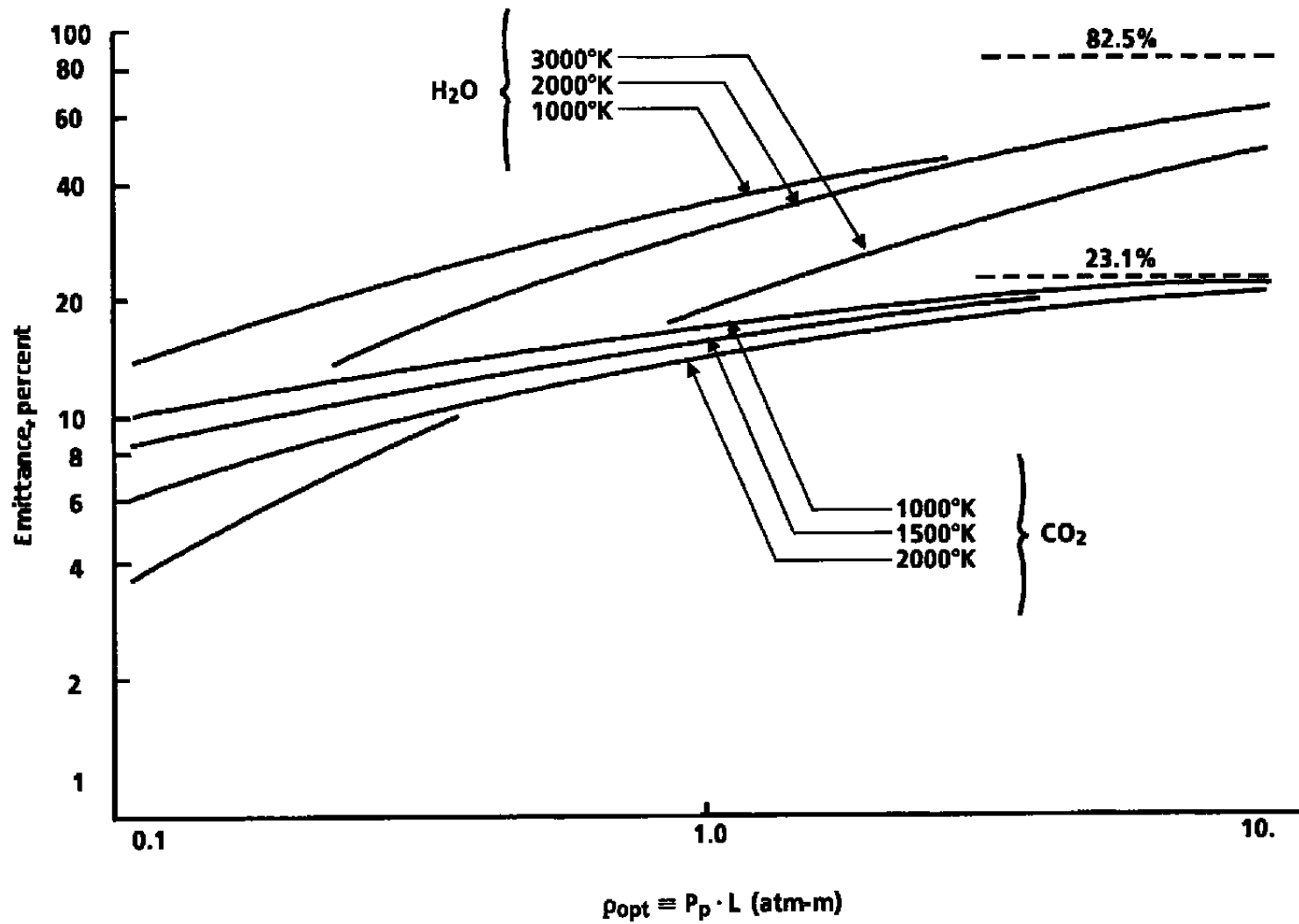
Figure 4. Total emittances of H_2O and CO_2 at 1 atm.
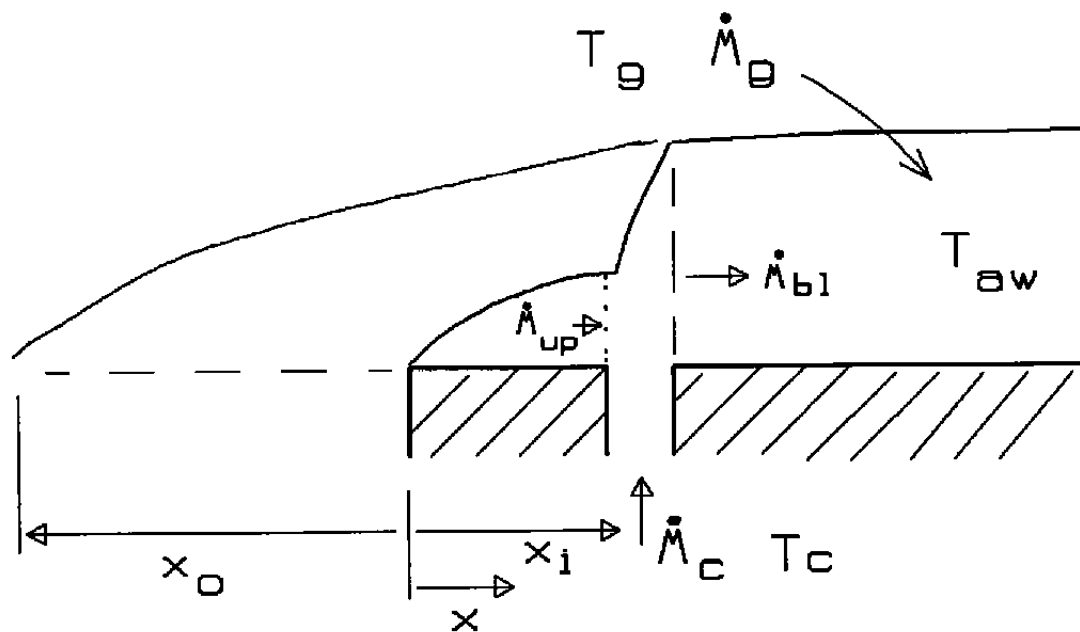
Figure 5. Gaseous film cooling analysis.
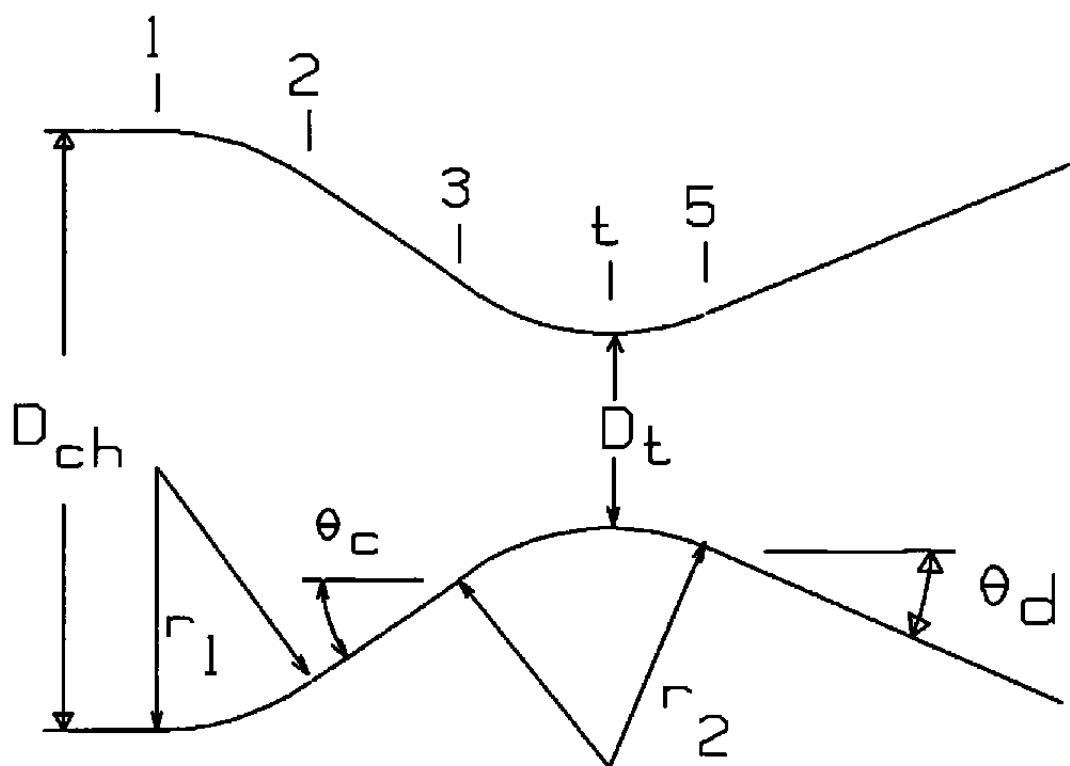
Figure 6. Chamber contour parameters.
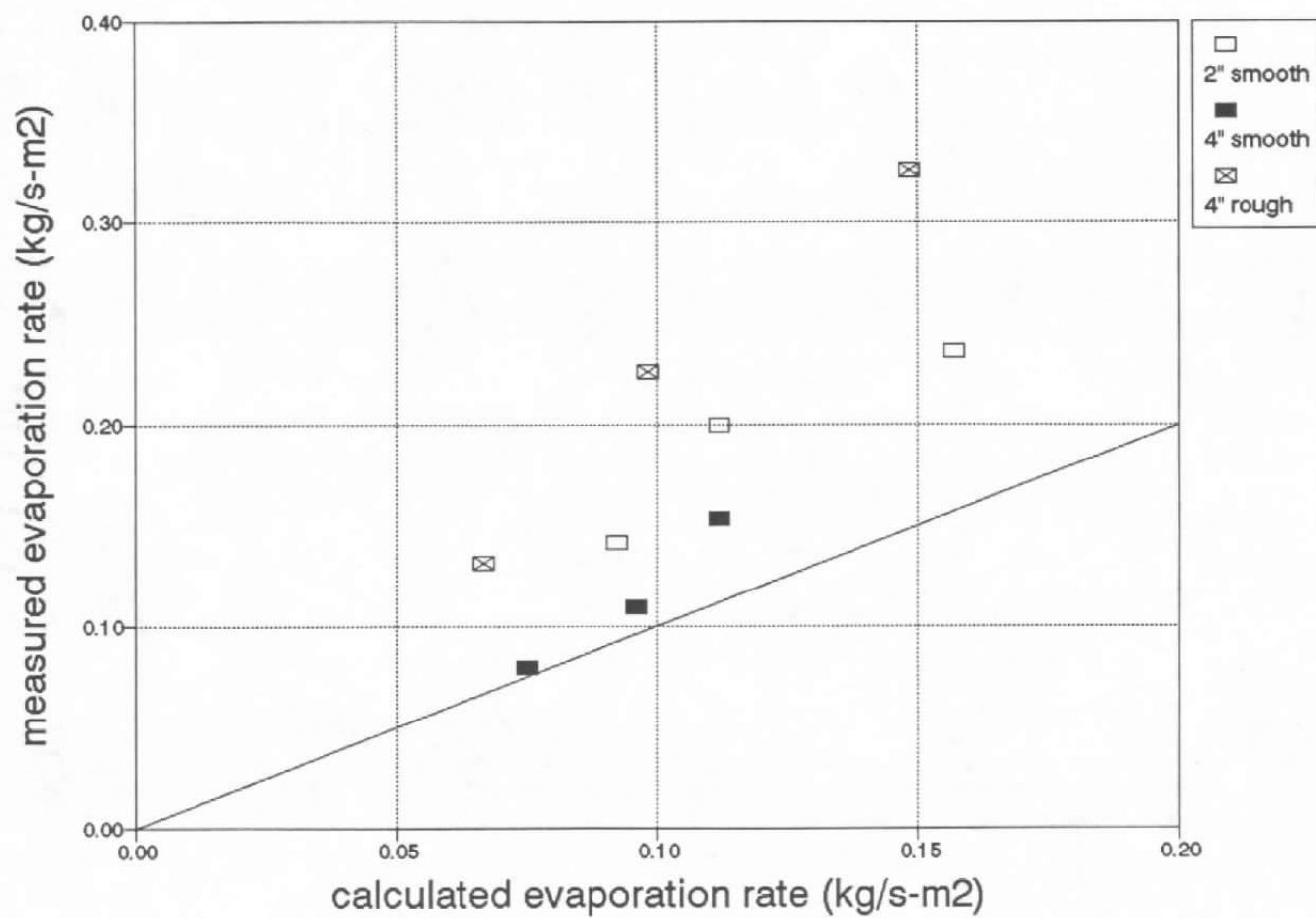
Figure 7. Comparison with data of G. R. Kinney, et al.
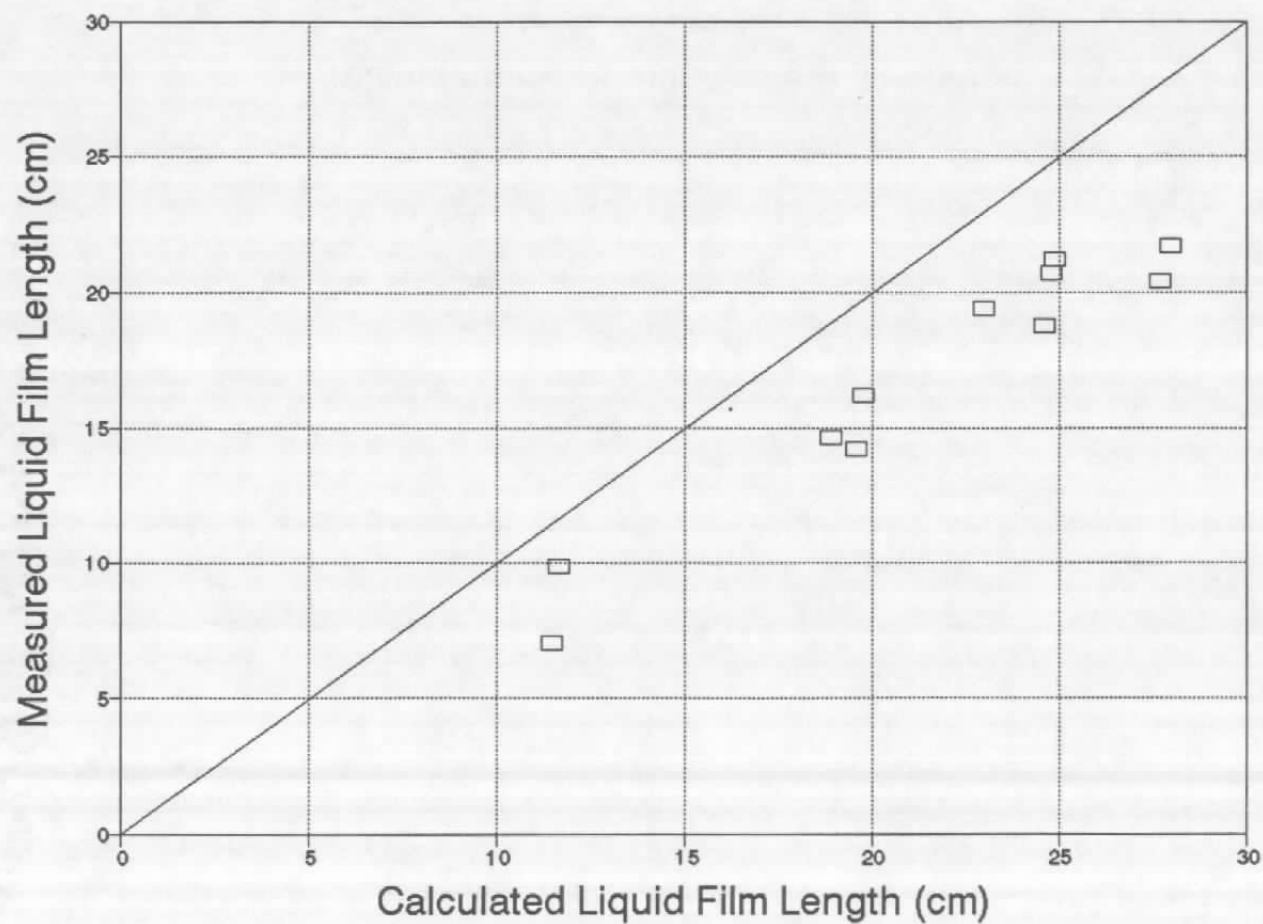
Figure 8. Comparison with data of G. Morrell.
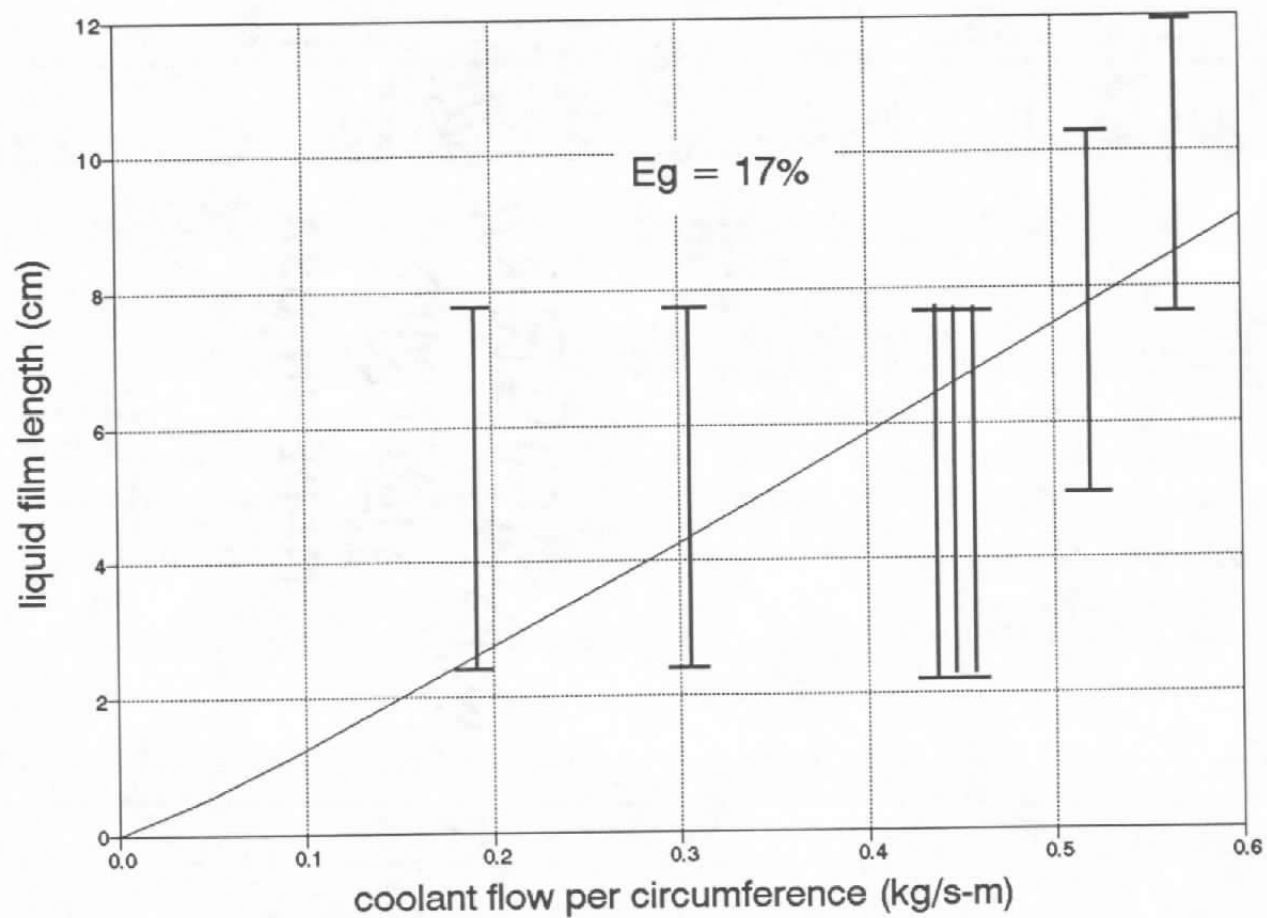
Figure 9. Comparison with data of R. C. Kesselring, et al.
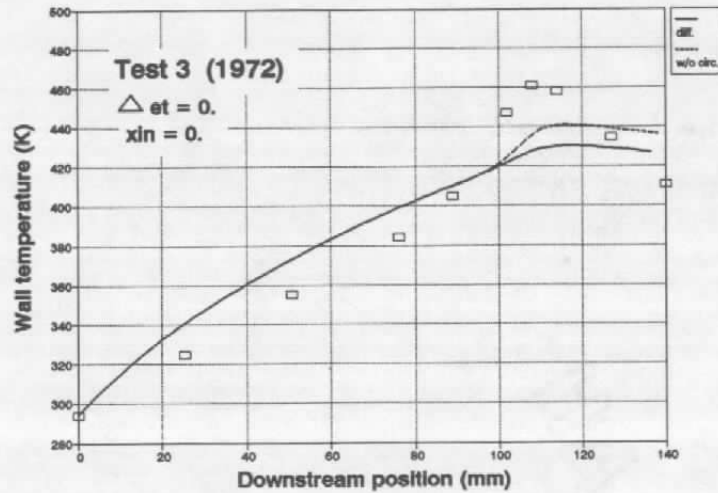
a. Test 3 (1972), Δet = 0, xin = 0
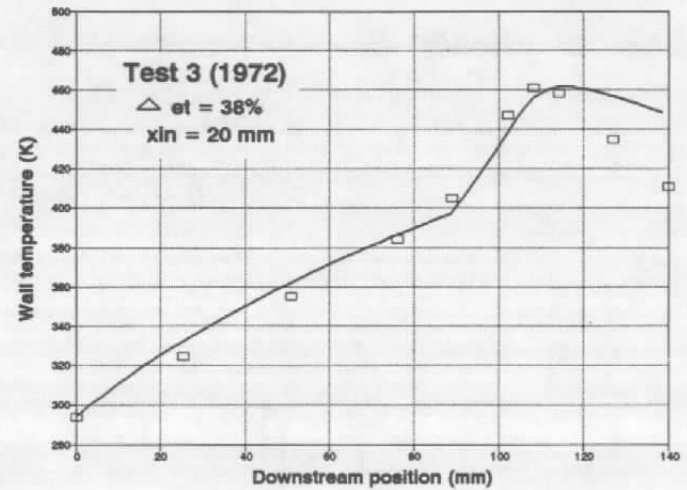
b. Test 3 (1972), Δet = 38%, xin = 20 min
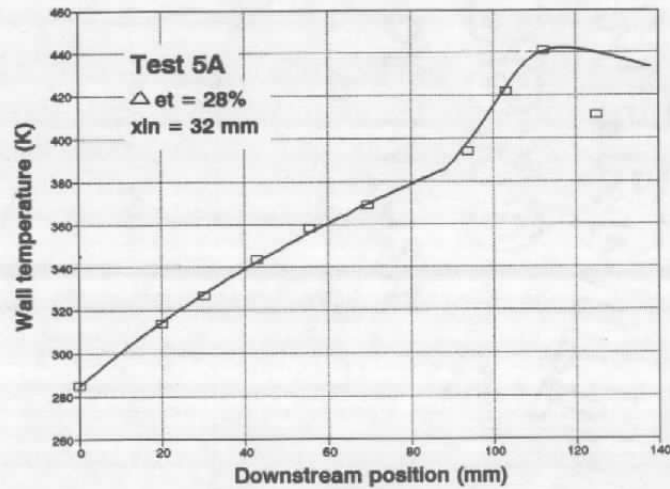
c. Test 5A, Δet = 28%, xin = 32 mm
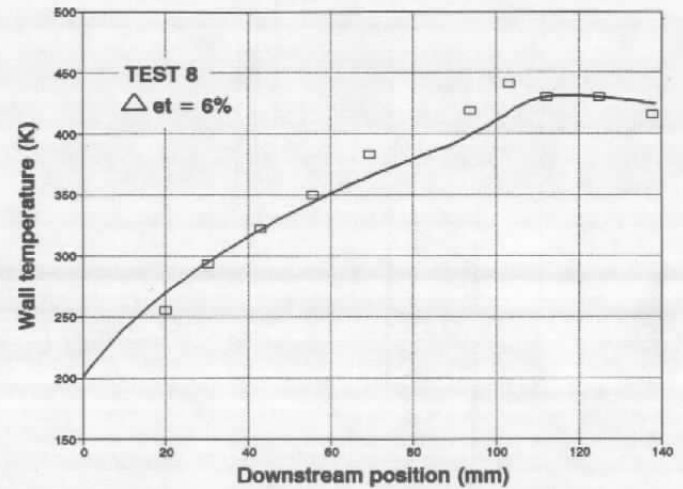
d. Test 8, Δet = 6%

Figure 10. Comparison with data of Ewen and Rousar.
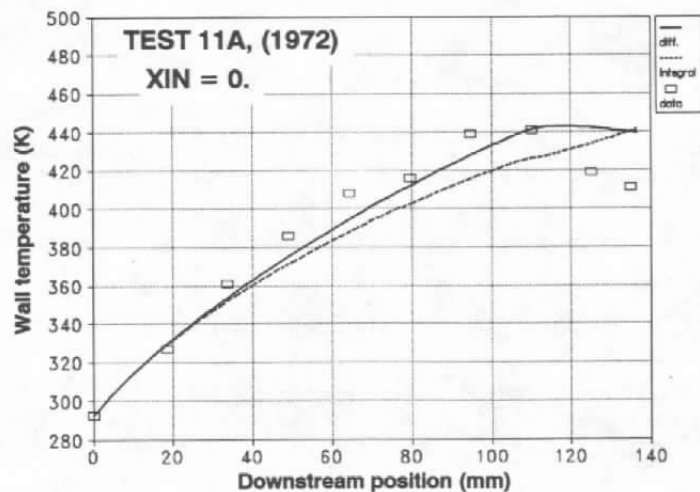
e. Test 11A (1972), xin = 0
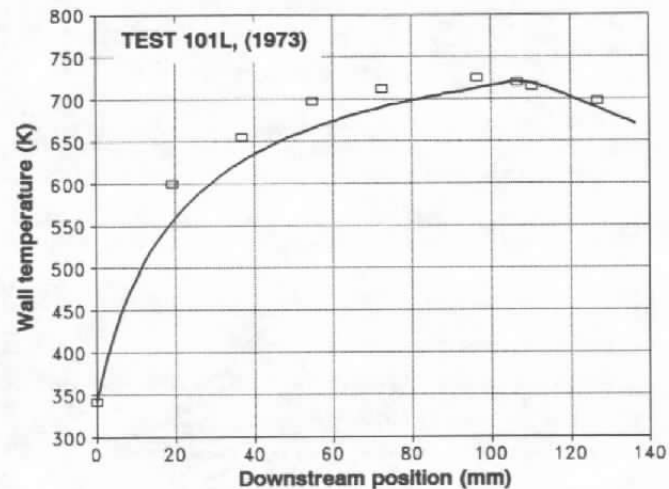
f. Test 101L (1973)
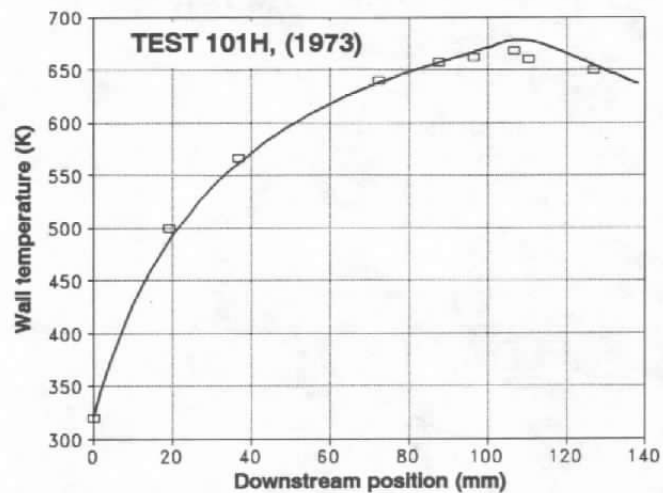
g. Test 101H (1973)
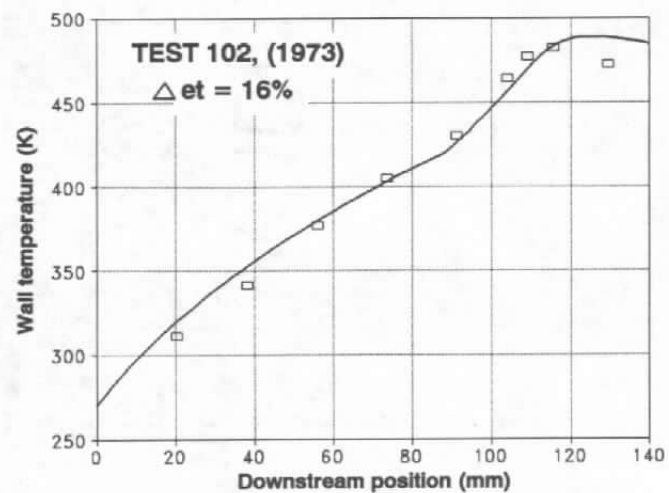
h. Test 102 (1973), $\triangle$et = 16%

Figure 10. Continued.
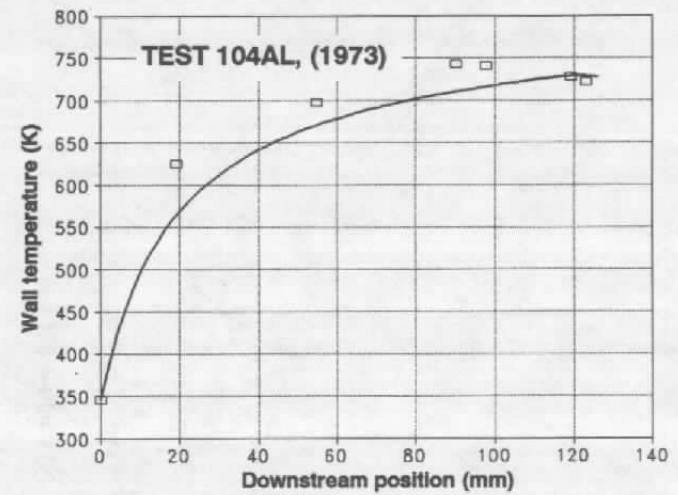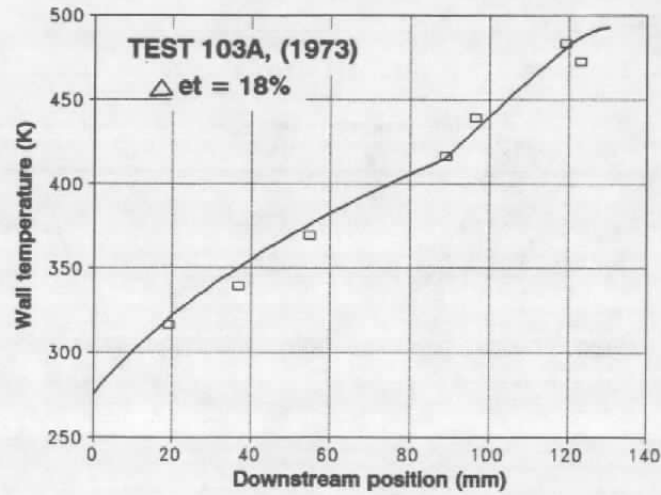
i. Test 103A (1973), Δet = 18%
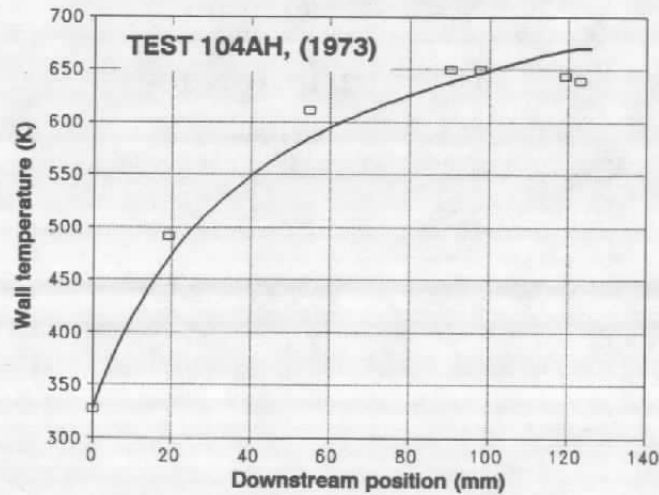
j. Test 104AL (1973)

k. Test 104AH (1973)
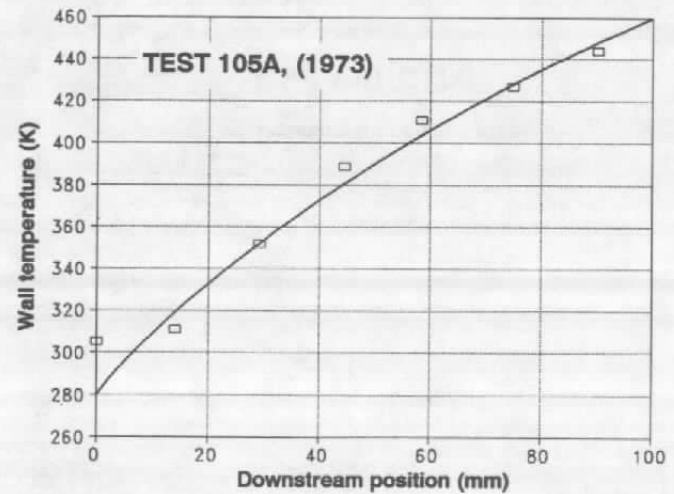
l. Test 105A (1973)

Figure 10. Continued.
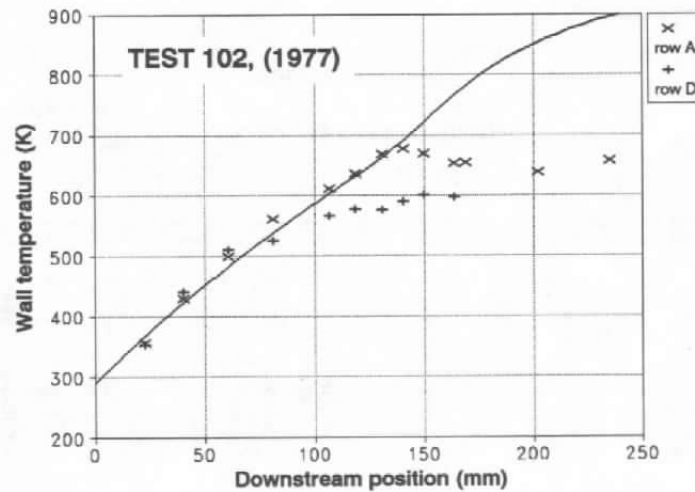
m. Test 102 (1977)
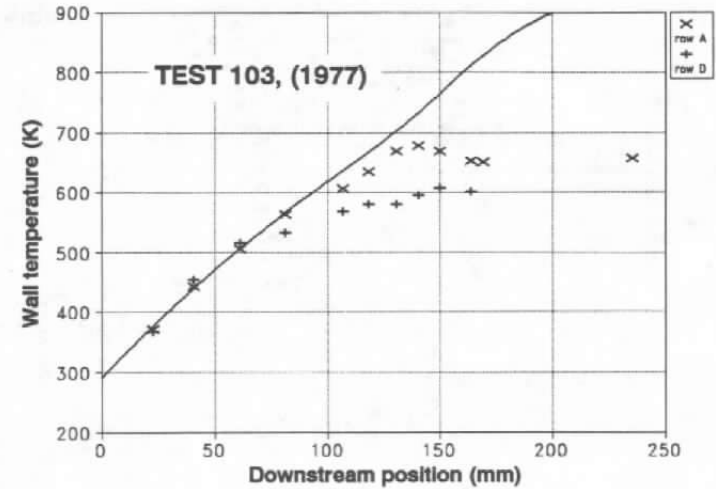
n. Test 103 (1977)
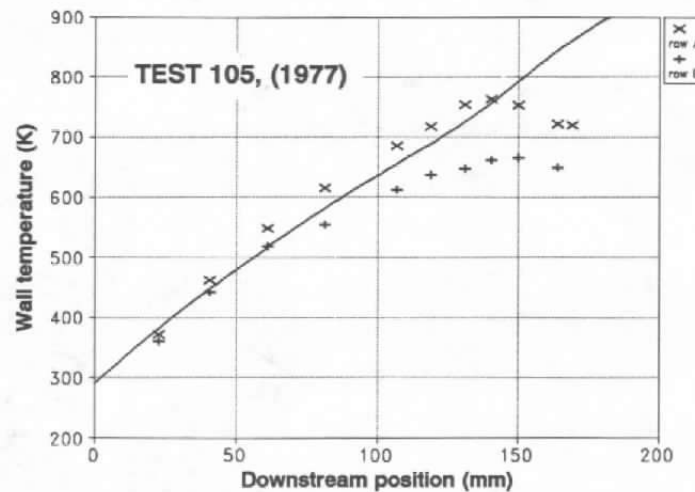
o. Test 105 (1977)
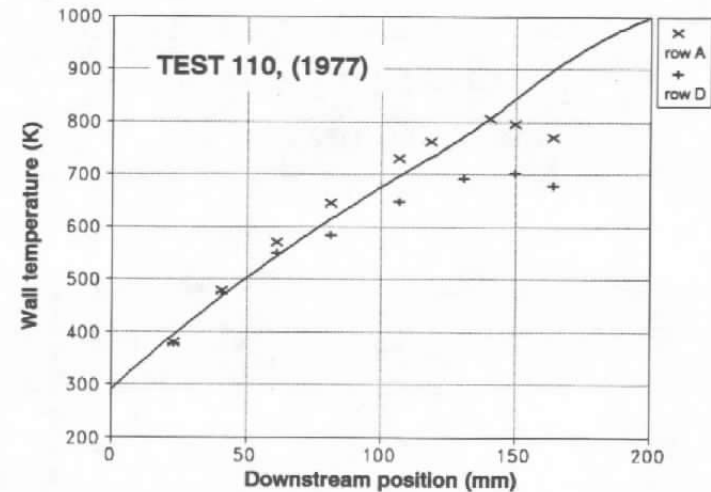
p. Test 110 (1977)

Figure 10. Continued.
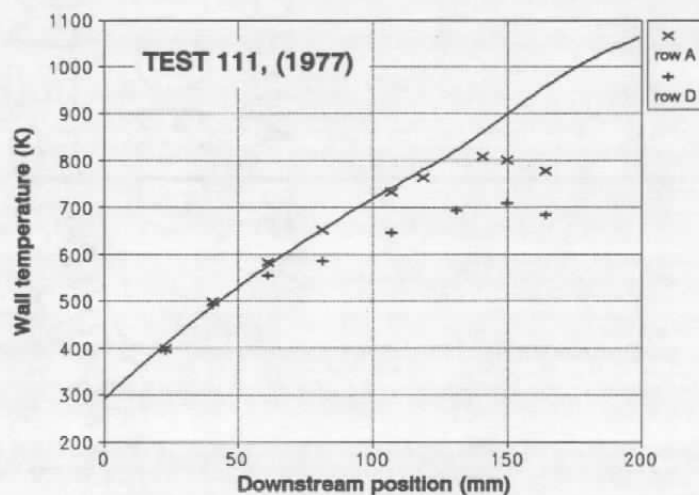
q. Test 111 (1977)
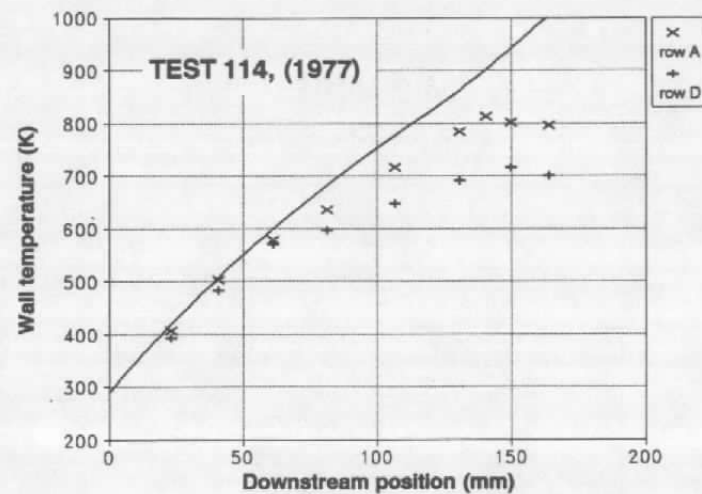
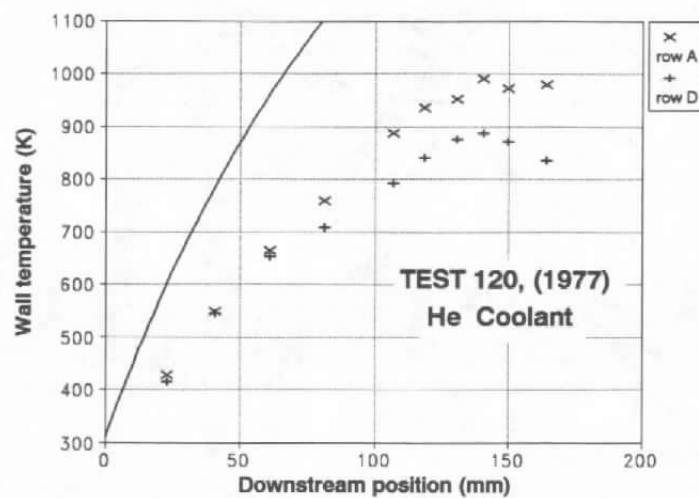r. Test 114 (1977)
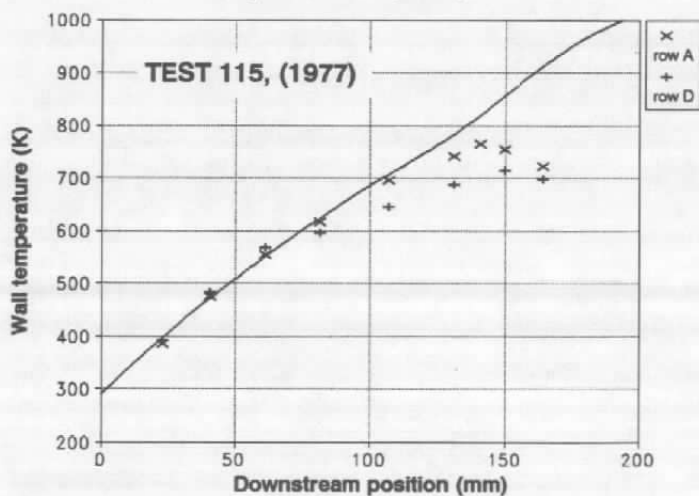
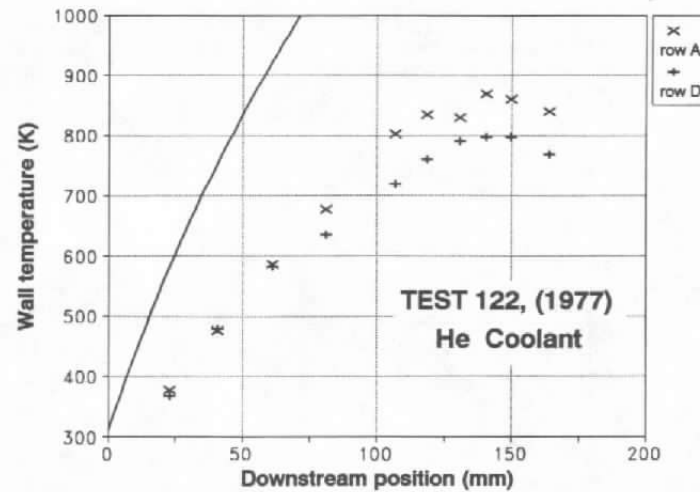s. Test 115 (1977)
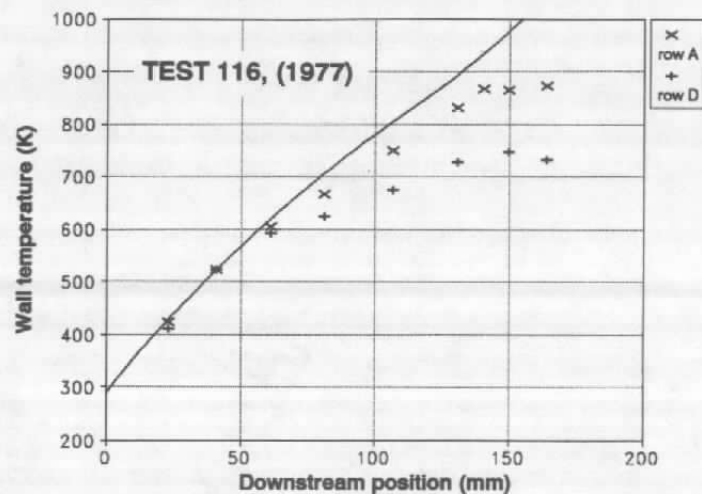
t. Test 116 (1977)

Figure 10. Continued.
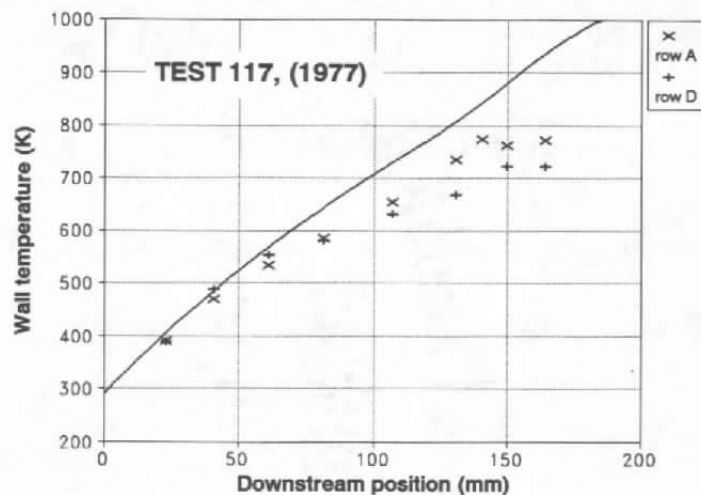
u. Test 117 (1977)
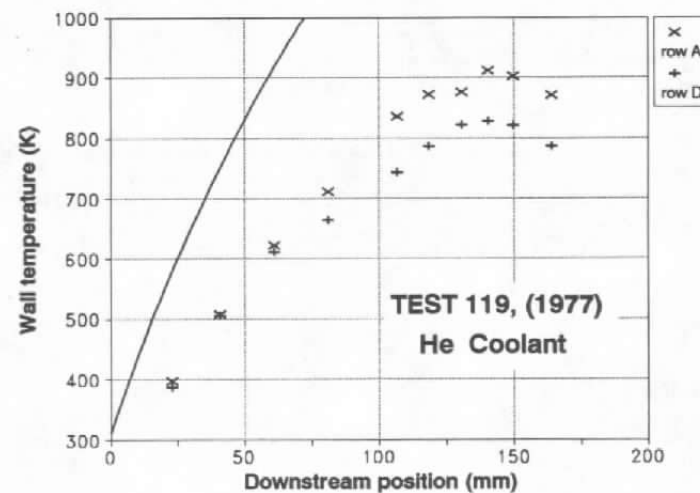
v. Test 119 (1977)

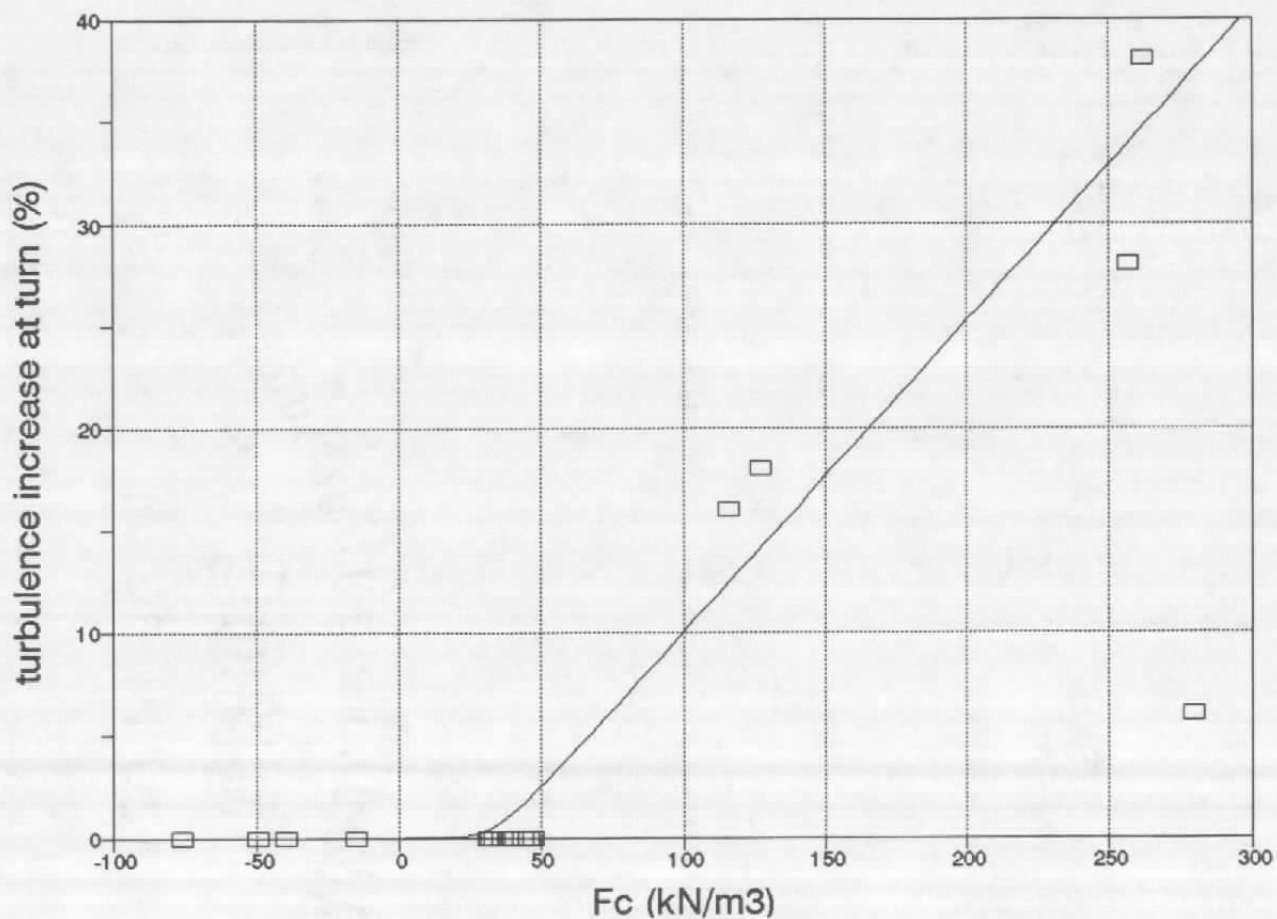w. Test 120 (1977)

x. Test 122 (1977)

Figure 10. Concluded.

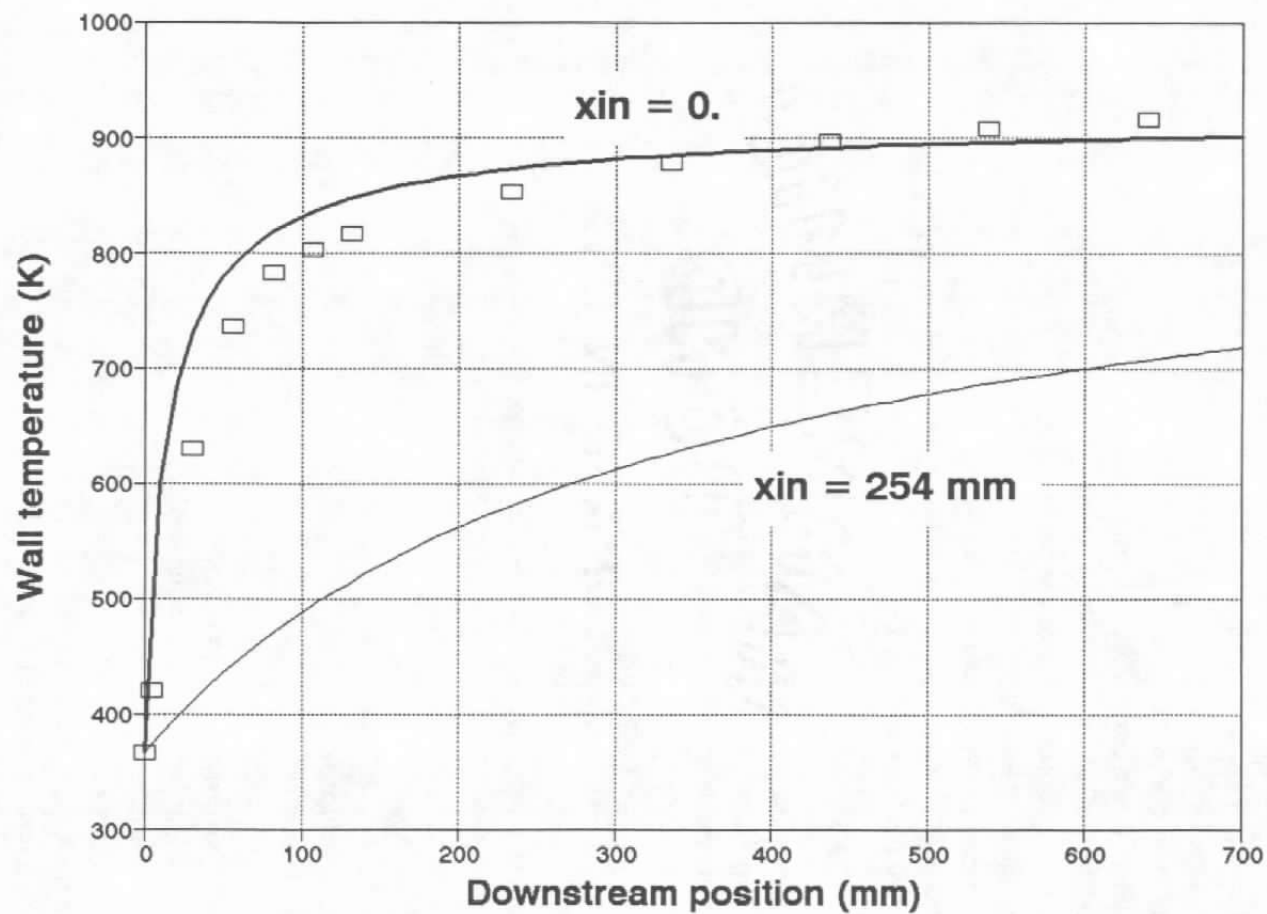Figure 11. Correlation of turn turbulence with centrifugal parameter.

Figure 12. Comparison with Kinney's Figure 4.

NOMENCLATURE

A = local cross-sectional area of chamber

A_w = absorptivity of chamber walls

C_f = skin friction factor = $2\tau_w/\rho_g U_g^2$

C_p = specific heat per mass

D = diameter of combustion chamber at position x

e_t = free stream turbulence intensity fraction

Δe_t = increase in turbulence due to converging turn

F = blowing parameter = m_v/G

G_{ch} = free stream gas mass flow per area = ρU_g

G_{mean} = mass flow at T_{mean} relative to liquid surface = $\rho_{mean}(U_g - U_l)$

h = convective heat transfer coeff.

H = F/St .

K = $G \mu_g^{0.25} / M_c^{1.25}$

K_g = thermal conductivity of free stream gas

K_M = correction factor for molecular weight

K_t = correction factor for turbulence

L = optical path length

L_{eff} = average optical path length

m_v = total liquid evaporation rate per surface area

M = molecular weight or

M_{bl} = boundary layer mass flow rate per circumference

M_c = gaseous coolant mass flow rate per circumference

n = no. of moles

N_c = mole fraction of CO_2

N_w = mole fraction of water vapor

Pr = Prandtl no of gas = $\mu_g C_{pg}/K_g$

P = absolute pressure

Q = heat flow per area

r = radius of convergence arc in nozzle

Re_D = Reynold's no based on diameter = GD/μ_g

St = Stanton no = $h/(G\,C_{pg})$

T = absolute temperature

T_c = temperature of liquid or gaseous coolant

T_v = saturation temperature of coolant

ΔT = $T_g - T_v$

U = axial velocity

x = distance from injection point (along contour)

x_e = x corrected for developing pipe flow

X = dimensionless distance = K x

y = distance from wall

Greek Symbols:.

γ = C_p/C_v = specific heat ratio

δ = boundary layer thickness

ϵ = gas emissivity

η = film cooling effectiveness

Γ = liquid coolant mass flow rate per circumference

λ = latent heat of vaporization of coolant

λ^* = $\lambda + C_{pl}(T_v\text{-}T_c)$

μ = dynamic viscosity

ρ = mass density

ρ_{opt} = optical density = P L

σ = surface tension of coolant or Stephan's const.

subscripts:

aw - adiabatic wall

bl - boundary layer

bo - burnout point

c - coolant, (liquid or gaseous)

ch - values in cylindrical chamber section

conv - convective

cr - at transition to "large waves"

g - free stream gas

l - liquid coolant

mean - mean temperature between free stream gas and liquid

o - for "dry-wall" conditions, without transpiration

rad - due to radiation

up - upstream

v - vapor

w - evaluated at wall